DESIGN AND FABRICATION
OF A SOLVENT RESISTANT MICROFLUIDIC DEVICE
FOR USE IN COMBINATORIAL SOLVENT ANNEALING STUDIES
OF BLOCK COPOLYMER THIN FILMS

by

Timothy D. Bogart

A thesis submitted to the Faculty of the University of Delaware in partial fulfillment of the requirements for the degree of Honors Bachelor of Chemical Engineering with Distinction.

Spring 2010

DESIGN AND FABRICATION

OF A SOLVENT RESISTANT MICROFLUIDIC DEVICE

FOR USE IN COMBINATORIAL SOLVENT ANNEALING STUDIES

OF BLOCK COPOLYMER THIN FILMS

by

Timothy D. Bogart

Approved: _____

Thomas H. Epps, III, Ph.D.
Professor in charge of thesis on behalf of the Advisory Committee

Approved: _____

Eric M. Furst, Ph.D.
Committee member from the Department of Chemical Engineering

Approved: _____

Norbert Mulders, Ph.D.
Committee member from the Board of Senior Thesis Readers

Approved: _____

Alan Fox, Ph.D.
Director, University Honors Program

ACKNOWLEDGMENTS

I would sincerely like to thank my advisor, Thomas Epps, for providing me the opportunity to learn and grow in a research environment, allowing me the freedom to make this project my own, and for challenging me intellectually every step of the way. His support and guidance allowed me to reach new heights as a both a person and a scientist. Maybe one day he'll let me win an argument.

I would especially like to thank my graduate student mentor, Julie Albert. Her never-ending support, guidance, and encouragement made it possible for me to continue when I lost the drive. There simply aren't enough words to describe how wonderfully amazing she has been the past two years and I am forever grateful to have had the privilege to know her as person. I hope she can finally take my advice and go home to relax now that I'm no longer around to worry her.

I would also like to thank Kelly Schultz for allowing me to use her UV setup, Elizabeth Kelly for being awesome and helping me run ^{1}H-NMR samples when time was running out, Kai Mayeda for just being handsome and funny making the time spent in lab more enjoyable, Maeva Tureau for being silly and entertaining making this whole experience more enjoyable, Wen-Shiue Young for sharing his culture in the form of tasty treats.

Lastly there's Sarah Mastroianni. Her non-stop sass, bantering, and hilarious attitude constantly distracted me from my work and in no way furthered my productivity and I thank her for that.

TABLE OF CONTENTS

LIST OF TABLES

LIST OF FIGURES

ABSTRACT

Block copolymer thin film phase behavior from self-assembly is significantly affected by the free surface energetics of the film and block interactions. Solvent vapor annealing promotes self assembly by lowering the glass transition temperature of the block copolymer below the ambient temperature while controlling the free surface energy and mitigating block interactions with solvent selection. Different thin film morphologies, which can be used in applications from nanotemplating to nanoporous membranes, can be produced by adjusting the solvents used in solvent vapor annealing. Solvent composition gradients enable high throughput studies of solvent effects on the phase behavior of block copolymer films.

A solvent resistant microfluidic device to create solvent vapor composition gradients was fabricated using selective photopolymerization techniques. The device was tested by creating a composition gradient of n-hexane and tetrahydrofuran (THF) for the solvent vapor annealing of a poly(styrene-*b*-isoprene-*b*-styrene) thin film. The composition gradient was characterized by ^{1}H-NMR and the phase behavior of the polymer film was analyzed using atomic force microscopy and optical microscopy. It was found, as expected, that as the solvent composition shifted from n-hexane to THF the phase behavior of the polymer film shifted from a mixed morphology to well ordered parallel cylinders prior to dewetting, demonstrating that the device performed as intended. The microfluidic device and methods developed here for solvent vapor annealing and analysis will be used to explore solvent effects on thin film phase behavior for different block copolymer systems.

Chapter 1

INTRODUCTION

1.1 Background

A block copolymer consists of two or more chemically distinct polymeric chains (blocks) covalently bonded to each other. Linear block copolymers are classified based on the number of blocks and number of different monomers present. An ABC triblock is comprised of three distinct polymer blocks each composed of a different monomer unit, whereas an ABA triblock is comprised of three distinct polymer blocks in which the end blocks are composed of the same monomer type (see Figure 1.1-1). In each case, thermodynamic incompatibilities between blocks cause segregation on the molecular scale (5 – 100 nm). This microphase separation produces complex morphologies that can be utilized in a number of applications from nanotemplating[1-7] to nanoporous membranes[8-11].

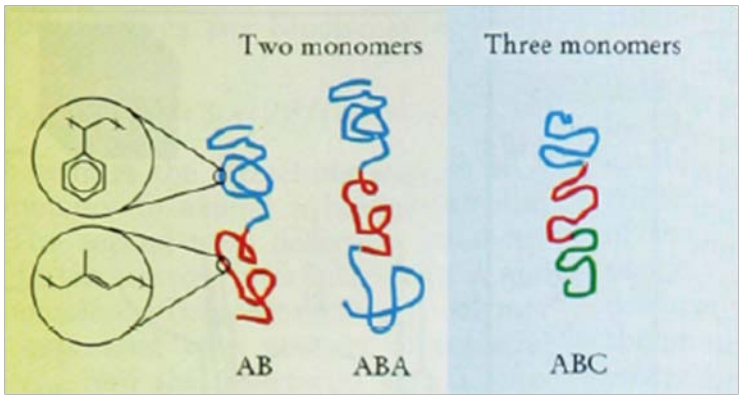

Figure 1.1-1 Representation of AB diblock, ABA triblock, and ABC triblock copolymers. Each colored strand represents a polymer block composed of a linear sequence of same-type monomers. The left inset shows two representative monomer chemical structures, poly(styrene) (top) and poly(isoprene) (bottom), with the diameter of the circle showing the typical monomer length scale. Image reproduced from Bates, F.S. and Frederickson, G. H. (1999) *Physics Today.* 52 32-38.

In bulk material, the microphase separation is governed by the interactions between the immiscible blocks. In the simple case of the AB diblock copolymer, phase behavior is controlled by three parameters: the degree of polymerization (N), the volume fraction composition (*f*), and the A–B Flory–Huggins interaction parameter (χ), which characterizes the immiscibility of the two blocks and is dependent upon the block chemistry and temperature ($\chi \propto T^{-1}$).[3] The overall segregation strength is determined by the product χN. Figure 1.1-2 shows a theoretical phase diagram for a diblock copolymer as a function of composition (*f*) and segregation strength (χN). The phase diagram shows several distinct morphologies for the diblock copolymer depending on the block copolymer composition and temperature including spheres in a

body centered cubic (BCC) lattice, cylinders in a hexagonal lattice, gyroid, and lamellae.[3] These same morphologies are also observed for symmetric ABA triblock copolymers.

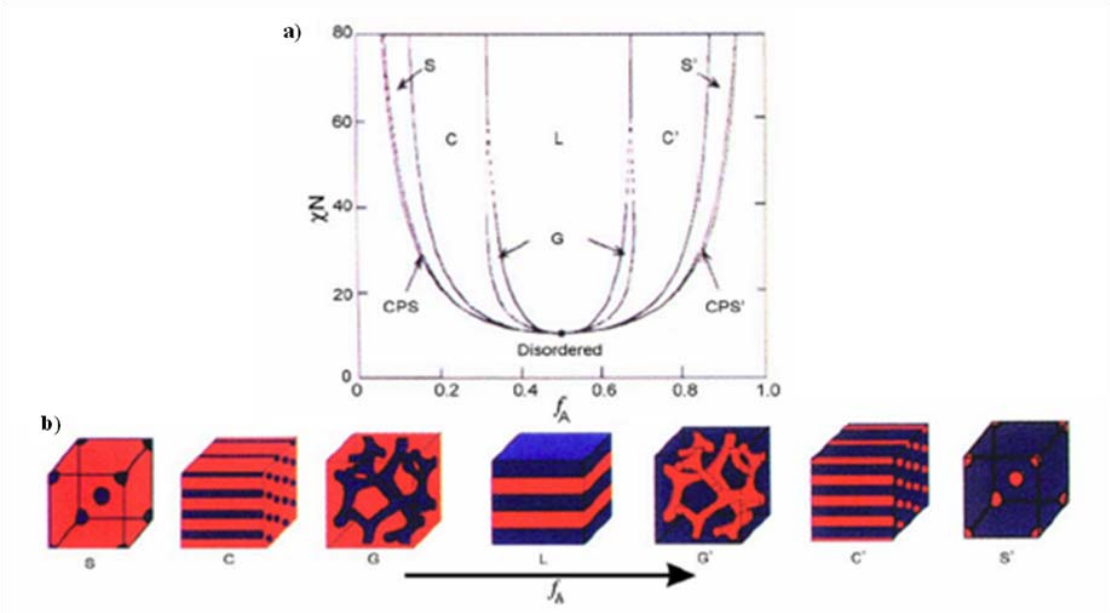

Figure 1.1-2 (a) Self-consistent mean-field theory[13] predicts the following equilibrium morphologies: spherical (S, S'), cylindrical (C, C'), gyroid (G, G'), lamellar (L) and close packed spheres (CPS, CPS'), depending on the composition, *f*, and segregation strength, χN. (b) Representations of the equilibrium microdomain structures as f_A is increased for fixed χN, with A and B blocks located in the blue and red regions, respectively. Image reproduced from Bates, F.S. and Frederickson, G. H. (1999) *Physics Today.* 52 32-38.

When confined to thin films, the lamellar and cylindrical domains form with a particular orientation to the substrate surface as shown in Figure 1.1-3. This orientation is particularly important for lamellae and cylinders because applications for the two differ considerably with domain orientation. For example parallel

cylinders can be used to template nanowires while perpendicular cylinders can be used for nanoporous membranes. As a result, the ability to understand and control the formation and orientation of domains and domain morphologies has become increasingly important.

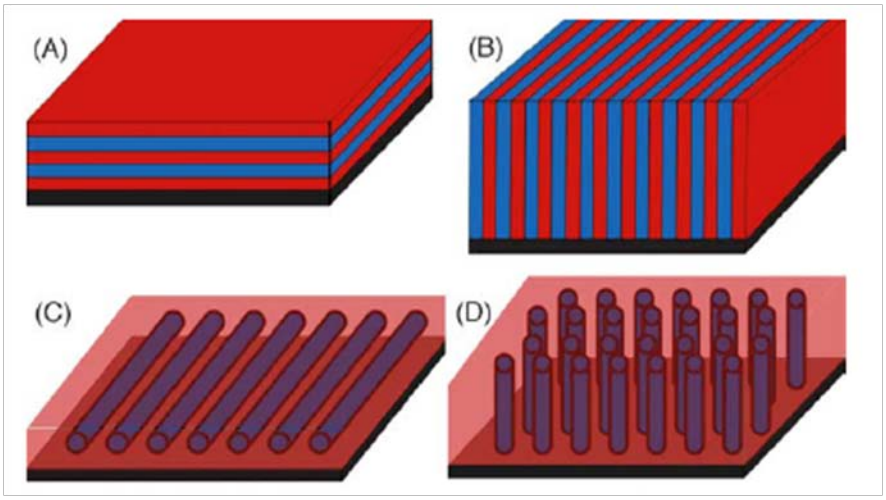

Figure 1.1-3 When confined to a thin film, the lamellar and cylindrical block copolymer domains form different orientations with respect to the substrate surface: (A) lamellae lying parallel to the substrate, (B) lamellae aligned perpendicular to the substrate, (C) cylinders aligned perpendicular to the substrate, and (D) cylinders aligned perpendicular to the substrate. Image reproduced from Segalman, R. A. (2005). *Materials Science and Engineering: R: Reports* 48(6): 191-226.

The orientation of a block copolymer thin film depends on film thickness and surface energy with the driving force being energy minimization of the system. The domains formed by microphase segregation occur on a nanometer lengthscale that is determined by the composition and degree of polymerization of the polymer system. If the film thickness is commensurate with the domain spacing then the morphology is

likely to be parallel to the substrate surface. In cases where the film thickness is not commensurate, the morphology may orient parallel or perpendicular depending on surface energetics. [12,28,29]

The substrate surface energy and the free surface energy also influence the orientation of a block copolymer thin film. If the surface is preferential for one of the blocks, then that block will migrate to that surface forming a wetting layer during self assembly. This wetting layer can occur at either the substrate surface or the free surface and may alleviate film thickness constraints for the polymer film, allowing for a parallel orientation of the block copolymer. If the surface is nonpreferential (neutral), then no wetting layer is formed. Therefore neutral surfaces are desirable for inducing perpendicular orientation and preferential surfaces are desirable for inducing parallel orientation.[29]

The two primary methods for altering the free surface energy during polymer film self assembly are thermal annealing and solvent annealing. In thermal annealing, a block copolymer film is heated to a temperature above its glass transition temperature thereby providing mobility to the polymer chains to promote self assembly. The free surface energy is controlled by the temperature at which the film is annealed and the atmospheric conditions above the polymer film.[3,14,15] Thermal annealing, however, is limited to polymers that do not degrade at high temperatures. In solvent annealing, solvent vapor swells the film and lowers the glass transition temperature of the block copolymer to below ambient temperature, providing mobility to the polymer chains to promote self assembly.[16,19] The free surface energy[20-27] and the rate of self-assembly are determined by the type and concentration of the solvent respectively. Additionally, solvent in the film affects the interactions between blocks,

and potentially, the relative volume fractions, which can lead to changes in morphology.[20, 22-27] Because solvent annealing can be performed at room temperature, it is an excellent method for annealing films that degrade at elevated temperatures.[28]

One of the methods for solvent annealing block copolymer thin films shown in Figure 1.1-4.[28] Two solvent bubblers are filled with the desired solvents. For annealing with a single solvent, the second bubbler is left empty. A gas cylinder provides nitrogen gas that flows through the solvent bubblers, enriching the nitrogen with solvent. The enriched streams join prior to entering the annealing chamber containing the polymer film. The polymer film absorbs some of the solvent from the vapor as the rest exits via a ventilation port. Typical annealing times are on the order of several hours depending on the block copolymer and solvent used. When annealing with one solvent, the concentration of solvent vapor above the film can be controlled by adjusting the flowrate of solvent enriched nitrogen relative to the pure nitrogen line. When annealing with two solvents, the solvent composition can be controlled by adjusting the relative flowrates while the overall concentration can be controlled by adjusting the total flowrate. This setup allows us to understand the effects of solvent composition and concentration on the self-assembly of block copolymer thin films.

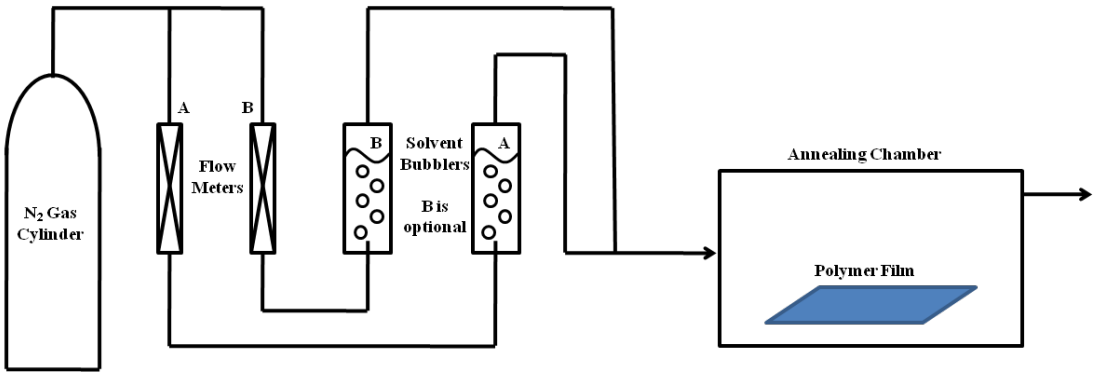

Figure 1.1-4 Schematic of setup used for solvent annealing of polymer films. Nitrogen flows through the solvent bubblers at volumetric flowrates specified by the flow meters. Nitrogen saturated with solvent enters the annealing chamber, annealing the polymer film.

With hundreds of annealing conditions to be explored for each block copolymer system, the ability to test multiple conditions simultaneously is a necessity. This work focuses on the design and fabrication of a solvent resistant microfluidic device to add to the current system to allow for simultaneous annealing under different solvent mixture compositions. The device acts as a mixing tree for solvent vapors to create chambers of different solvent compositions for simultaneous annealing.

Chapter 2

DEVICE FABRICATION

The microfluidic device was fabricated in three steps. First, a transparent mask of the design was created. Second, the mask was used to create a raised master template of the design for imprinting. Third, the master template was used to pattern the channels into the final device.

2.1 Transparent Mask Design

The design of the device was based on a simple branching tree as shown in Figure 2.1-1. Two solvent streams enter the device through injection ports, diffuse through the mixing tree, and enter the annealing chambers at the end. The branching tree allows the two solvents to mix, creating different solvent compositions in each of the annealing chambers. Chambers 1 and 6 consist of nearly pure solvents A and B, respectively, while chambers 2 through 5 contain a mixture of the two solvents; chambers 2 and 3 have higher concentrations of A while chambers 4 and 5 have higher concentrations of B. Chamber 7 is not connected to the branching tree and is used as a control to show that solvent does not penetrate through the walls of the chambers.

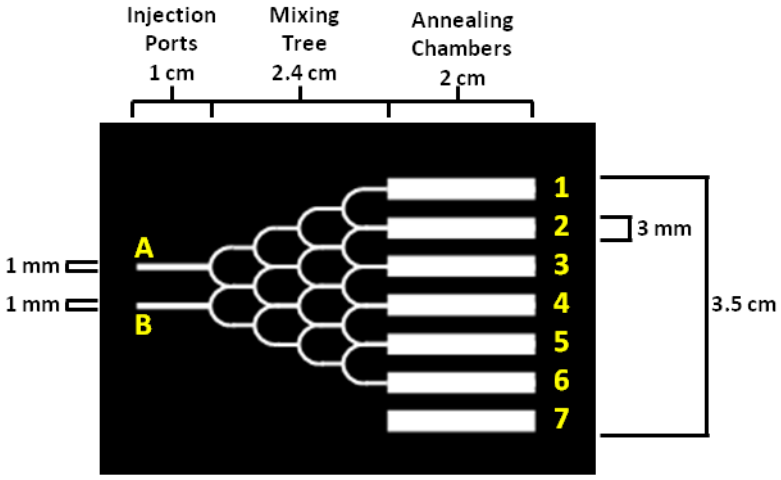

Figure 2.1-1 The branching tree design mask for the solvent annealing microfluidic device. Nitrogen enriched with solvents A and B enter through their respective injection ports via syringe needles (21 G). The solvent vapors mix through tree and enter the annealing chambers. A gradient of vapor compositions is formed with nearly pure A in chamber 1 and nearly pure B in chamber 6. Chamber 7 is not connected to the mixing tree and is used as a control.

A transparent mask of the design shown in Figure 2.1-1 was made by printing the mask onto two transparencies. The transparencies were cut to size (50 mm x 75 mm) and overlaid such that the design overlapped perfectly. The two transparencies were secured together and mounted onto a 50 mm x 75 mm x 1 mm glass slide using double sided tape.

2.2 Master Template

2.2.1 Process Overview

A frontal photopolymerization technique was used for the fabrication of the master template.[30,31] The technique uses ultra-violet (UV) light and the transparent mask of the design to selectively photopolymerize thiolene into a hard, raised template

of the design. A poly(dimethylsiloxane) (PDMS) spacer was used to confine the thiolene between glass slides for the photopolymerization. The photopolymerization occurs by the process shown in Figure 2.2-1. UV light breaks the sulfur hydrogen bond forming a thiol radical. The thiol radical subsequently attacks the vinyl functional group forming a sulfur-carbon bond and a vinyl radical. The radical chain transfers from the vinyl to the thiol group propagating the polymerization process. Radical termination occurs by radical-radical recombination.[32]

Step 1: Initiation $CH_2=CH\text{-}R\text{-}SH \xrightarrow{UV} CH_2=CH\text{-}R\text{-}S\cdot$

Step 2: Propogation $CH_2=CH\text{-}R\text{-}S\cdot + CH_2=CH\text{-}R\text{-}SH \rightarrow CH_2=CH\text{-}R\text{-}S\text{-}CH_2\text{-}C\cdot H\text{-}R\text{-}SH$

Step 3: Chain Transfer $H_2=CH\text{-}R\text{-}S\text{-}CH_2\text{-}C\cdot H\text{-}R\text{-}SH + CH_2=CH\text{-}R\text{-}SH \rightarrow CH_2=CH\text{-}R\text{-}S\text{-}CH_2\text{-}CH_2\text{-}R\text{-}SH + CH_2=CH\text{-}R\text{-}S\cdot$

Step 4: Termination $R\cdot + R'\cdot \rightarrow R\text{-}R'$

Figure 2.2-1 Photopolymerization mechanism for thiolene. (Step 1) UV radiation transforms the thiolene molecule into a thiol radical. (Step 2) The thiol radical attacks the ene function group of another thiolene molecule bonding the two together and creating a carbon radical. (Step 3) The radical then chain transfers to form another thiol radical propogating the polymerization reaction. (Step 4) Termination is the result of radical coupling.

2.2.2 PDMS Spacer Fabrication

Lids were removed from several model A203 plastic cases from Flambeau Cases for use as molds. The elastomer base and curing agent (Sylgard® 184 Silicone Elastomer) were mixed in a 10:1 ratio by weight and degassed by placing under

vacuum (-26 mmHg gauge) for 1 hour prior to pouring into the mold. The PDMS was cured overnight at 80 °C under atmospheric conditions. The result was several 8 in. x 4 in. x ¼ in. slabs of PDMS. A razor blade was used to cut 2 in. x 3 in. x ¼ in. rectangles of PDMS from the slabs. The center of each rectangle was removed leaving a ½ in. rectangular border, creating the spacers for the setup.

2.2.3 Photopolymerization of Master Template

Two glass slides were rinsed with ethanol and cleaned under UV ozone (UVO) for 30 minutes (Jelight Model 342, 28 mW/cm^2, 245 nm). After cleaning, the sandwich shown in Figure 2.2-2a was constructed. The PDMS spacer was placed on top of the UVO treated side of one of the glass slides and pressed firmly into place. Thiolene (Norland Optical Adhesive 81) was poured at room temperature into the center of the spacer until the level just started to exceed the height of the spacer. The second glass slide was placed, with the UVO treated side facing down, at a 45° angle to the end of the PDMS spacer and slowly lowered onto the spacer such that the slide came into full contact with the thiolene resin and no air bubbles were trapped inside the sandwich. Excess thiolene forced out of the cavity by the pressing of the glass slide was wiped away using acetone. The transparent mask was laid on top and the sandwich was placed under UV irradiation (Spectroline Model SB-100PD, 365 nm, 7.5 inches from lamp, 0.75 mW/cm^2) for 45 seconds.

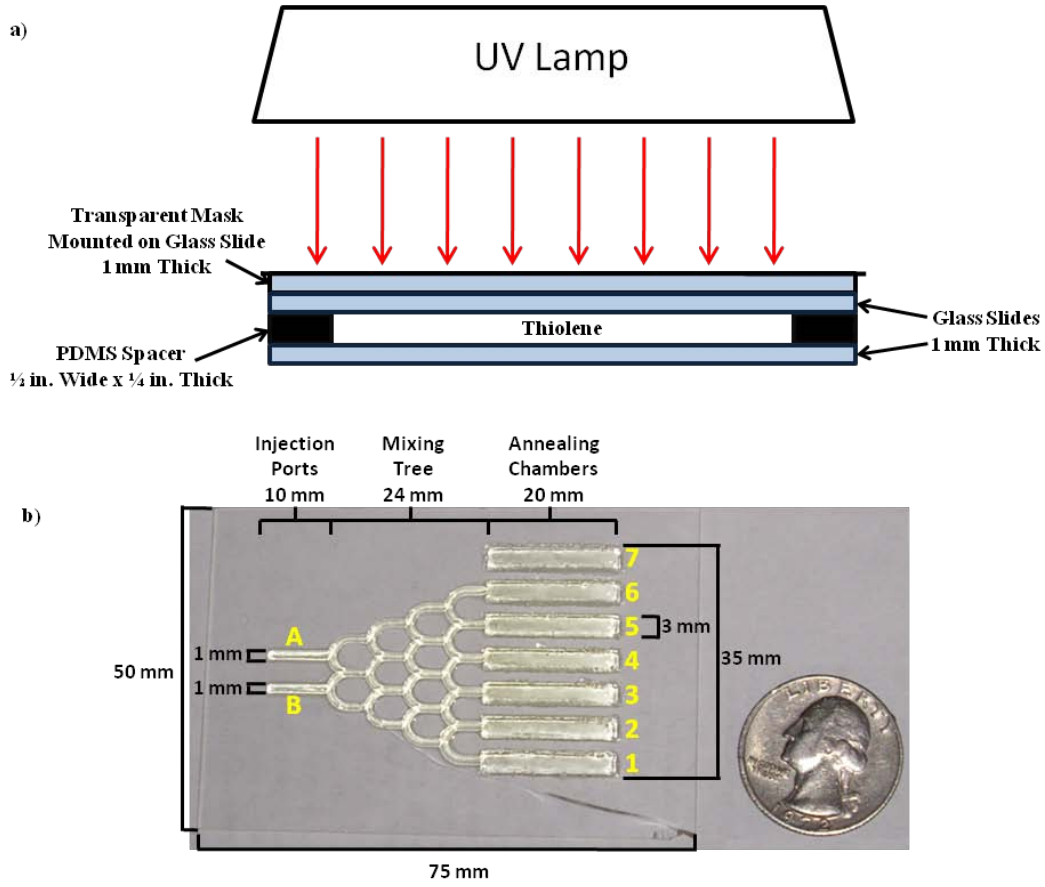

Figure 2.2-2 (a) Cross-sectional view of sandwich setup for master template fabrication. A PDMS spacer is used to separate two glass slides with thiolene filling the center of the device. The transparent design mask mounted on another glass slide is placed on top. UV light is used to irradiate the device from above selectively polymerizing the thiolene according to the design mask. (b) After irradiation the sandwich is opened and non-polymerized material is rinsed away leaving behind patterned ridges of the design approximately 750 µm in height.

After irradiation the upper glass slide was removed from the sandwich. The polymerized thiolene adhered to the upper glass slide along with some non-

polymerized thiolene. The bulk of the non-polymerized thiolene was rinsed from the slide using ethanol and a 2:1 mixture of ethanol and acetone. A razor blade, cotton swabs dipped in acetone, and an ethanol rinse were used to carefully remove the remaining non-polyerized thiolene without disturbing the polymerized pattern. Upon removal of the non-polymerized material, the template was placed under UV irradiation for 5 minutes (365 nm, 0.75 mW/cm^2) to increase the structural integrity of the ridges. The final master template had hardened ridges approximately 750 μm in height in the specified design as shown in Figure 2.2-2b.

2.3 Final Device Fabrication

Sartomer CN4000 fluorinated oligomer (CN4000), 1H,1H-Perfluoro-n-decyl acrylate (PFDA) (ExFluor), and 2,2-dimethoxy-2-phenylacetophenone photoinitator (Acros) were used as received. These materials were selected due to their solvent resistant properties after polymerization. A glass slide was rinsed with ethanol and cleaned under UVO for 30 minutes. After cleaning, the sandwich shown in Figure 2.3-1a was constructed using the cleaned glass slide as the top and the master template as the bottom with a PDMS spacer in between. Clamps around the sandwich provided a tight seal. A 2:1 mixture by weight of the PFDA:CN4000 with 0.15 weight percent photoinitiator was injected by syringe through the PDMS spacer into the hollow of the sandwich. The sandwich was placed under UV irradiation for 15 minutes (365 nm, 0.75 mW/cm^2), curing the fluorinated acrylate mixture.[33] Immediately following irradiation, the cured material was carefully removed from the sandwich and lifted off the master template. Uncured mixture was rinsed off using ethanol and water. The result was a stiff yet rubbery device with the desired channels imprinted as show in Figure 2.3-1b.

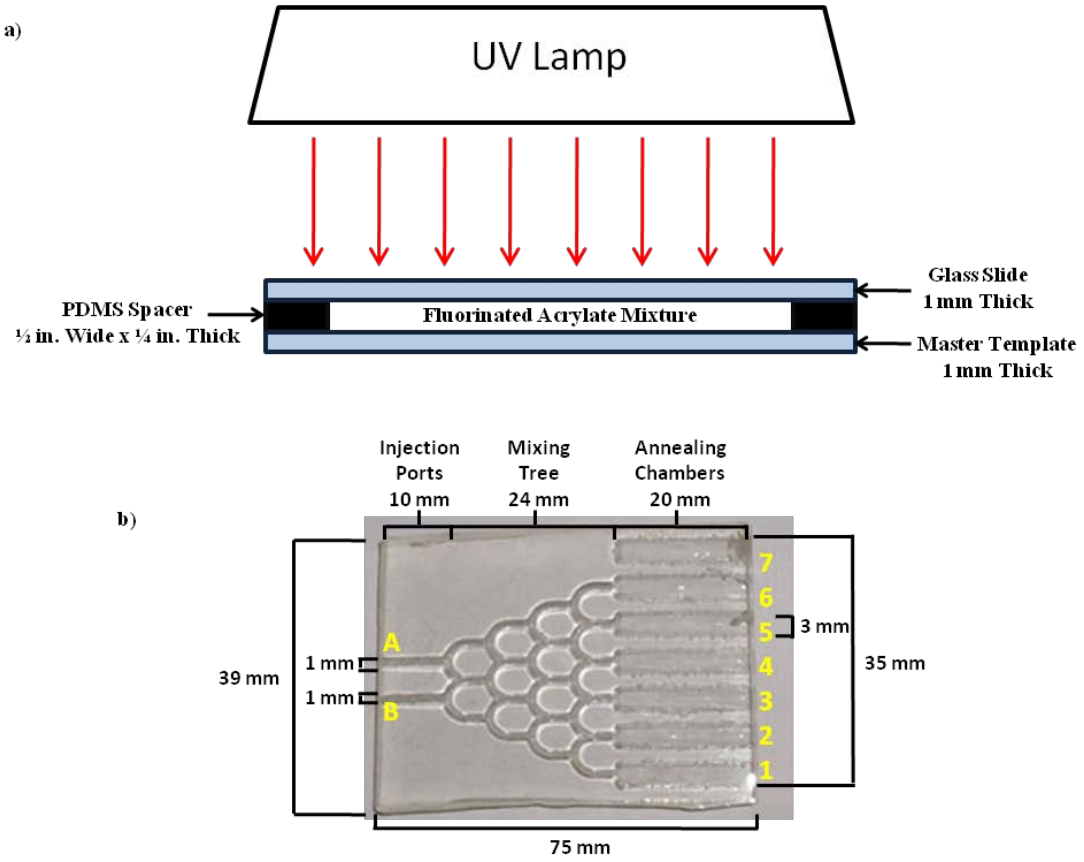

Figure 2.3-1 (a) Cross-sectional view of sandwich setup for final device fabrication. A PDMS spacer is used to separate a glass slide from the master template with a fluorinated acrylate mixture filling the center of the device. UV light is used to irradiate the sandwich from above curing the fluorinate acrylate mixture. (b) After irradiation the sandwich is opened and the device is removed from the master template resulting in patterned channels approximately 750 µm deep of the design

2.4 Solvent Vapor Collection Device

A second device was fabricated by the same processes described in sections 2.1 through 2.3 using the template shown in Figure 2.4-1. This design includes outlet

ports for connection via syringe needles (21G) to a series of cold traps for condensing the solvent vapors from each chamber for analysis.

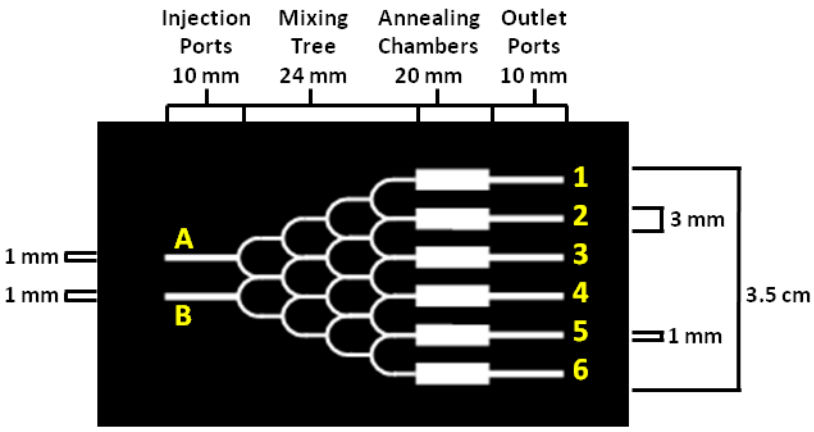

Figure 2.4-1 The branching tree design mask for the solvent collection microfluidic device. Nitrogen enriched with solvents A and B enter through their respective injection ports via syringe needles (21G). The solvent vapors mix through the tree and enter the annealing chambers. A gradient of vapor compositions is formed with nearly pure A in chamber 1 and nearly pure B in chamber 6. The solvent vapors exit the device through the outlet ports in each chamber via syringe needles (21G) for collection.

Chapter 3

SOLVENT ANNEALING AND SOLVENT COLLECTION

3.1 Polymer Thin Film Production

A 2 wt% solution of block copolymer in tetrahydrofuran (THF) was prepared and filtered for impurities using a 10 μm syringe filter. The solution was used to flowcoat[34] a 25 mm x 80 mm film onto a silicon substrate that was UVO cleaned for 30 minutes and rinsed with toluene. The film was divided into two 25 mm x 40 mm films for annealing with the microfluidic device.

3.2 Device Preparation

The device and polymer film were prepared for annealing as shown in Figure 3.2-1. The ends of the device were cut such that the injection ports and the annealing chambers became were accessible at their ends. The microfluidic device was placed with the channels facing down with the annealing chambers on the device overlapping the polymer film. Excess silicon wafer around the device was trimmed off for easier clamping. The device and substrate were sandwiched between two 50 mm x 75 mm x 1 mm glass slides and tightly clamped to ensure that there were no gaps between the device and the silicon wafer through which solvent vapor could diffuse. When performing solvent collection, the same sandwich was constructed using the solvent collection device, but without a silicon wafer.

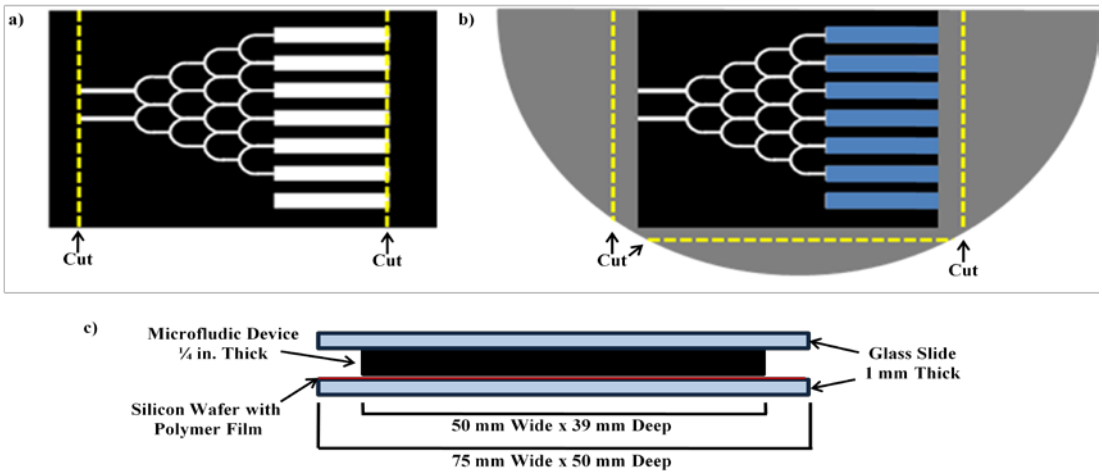

Figure 3.2-1 Preparation of the polymer film and microfluidic device sandwich. a) The ends of the microfluidic device were cut off to open the injection ports and annealing chambers to atmosphere. b) Device is placed on silicon wafer overlapping the polymer film (shown in blue) and excess silicon is trimmed away. c) Device and wafer is clamped tightly between a quartz plate and glass slide.

3.3 Solvent Annealing

The schematic for the solvent annealing setup is shown in Figure 3.3-1. A gas cylinder provided nitrogen gas (2.25 psig) through two separate lines (A and B) of solvent resistant fluoro-polymer lined tygon tubing. The nitrogen in each line flowed through a solvent bubbler at a rate (0-50 mL/min) controlled by flow meters, saturating the nitrogen with the respective solvent. The ends of the lines were connected to 1 mL syringes with syringe needles (21 G) attached. The needles were inserted into the injection ports on the device. The solvent enriched nitrogen streams flowed through the mixing tree, entered the annealing chambers, and exited the device through the openings at the ends of the chambers. Polymer films were annealed for 1 –

24 hours. The annealed polymer film was imaged using atomic force microscopy (AFM) to characterize the resulting morphologies.

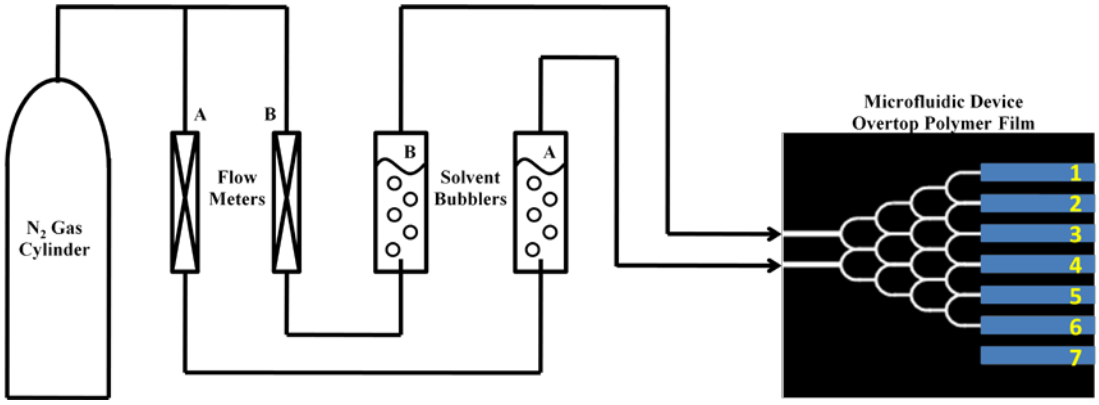

Figure 3.3-1 Schematic of setup used for solvent annealing of polymer films. Nitrogen flows through the solvent bubblers at volumetric flowrates specified by the flow meters. Nitrogen saturated with solvent enters the microfluidic device through the injection ports, mixes in the device, and anneals the polymer film.

3.4 Solvent Collection

The schematic for the solvent collection setup is shown in Figure 3.4-1, which is based on a simple condenser to extract the solvent mixture from the nitrogen gas. The setup is the same as that used for solvent annealing except the ends of the chambers were not open to the atmosphere. Instead syringe needles (21 G) were connected to both ends of solvent resistant tubing and inserted into the six outlet ports of the device. The other end of each of the tubes was connected to a 1.5 mL vial tightly sealed with a septum cap. A second syringe needle was inserted into each of the vials to create an open system. The vials were bundled together in a hexagonal pattern around an uncapped vial using rubber bands to provide stability. The vial

bundle was place in the center of a crystallization dish and wrapped in glass wool. The crystallization disk was placed on top of an inverted 50 mL beaker in a dry ice/isopropanol bath such that the isopropanol level did not rise above the sides of the crystallization dish. The dry ice bath was covered with glass wool for insulation. Solvent vapor was condensed in each of the vials and the composition was analyzed by proton nuclear magnetic resonance (^{1}H-NMR) using deuterated chloroform as the solvent.

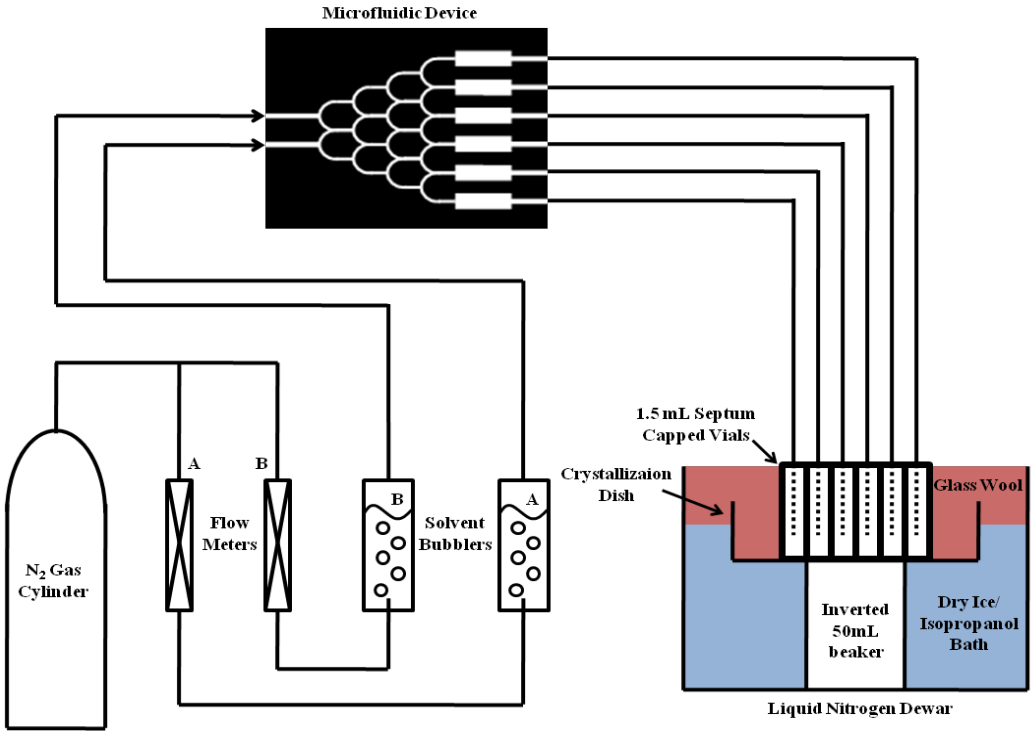

Figure 3.4-1 Schematic of setup used for solvent collection. Nitrogen flows through the solvent bubblers at volumetric flowrates specified by the flow meters. Nitrogen saturated with solvent enters the microfluidic device through the injection ports, mixes in the device, exits through the outlet ports, into individual vials, and is condensed.

Chapter 4

MICROFLUIDIC DEVICE TESTING

4.1 Testing Conditions

A symmetric block copolymer of poly(styrene-*b*-isoprene-*b*-styrene) (SIS) (Polymer Source SIS v4211) with a molecular weight of 118 kg/mol, block volume fractions of $f_s = 0.134$, $f_I = 0.732$, $f_s = 0.134$, and polydispersity index (PDI) of 1.09 was selected for annealing with the microfluidic device. Thin films were prepared by the methods described in Section 3.1. At this composition and molecular weight the as cast block copolymer film forms a mixed morphology of perpendicular and parallel poly(styrene) (PS) cylinders in a poly(isoprene) (PI) matrix.

Tetrahydrofuran (THF) and n-hexane were selected as annealing solvents. These solvents were chosen for the differences in polymer solubilities, THF is a good solvent for both blocks whereas n-hexane is a poor solvent for poly(styrene). My earlier work has shown that different orientations are produced when performing single component solvent anneals using these solvents with the SIS thin film. Solvent vapor annealing with THF for short periods of time (~1 hr) produced parallel cylinders with relatively long range order while annealing for longer times (>4 hours) resulted in the polymer film dissolving (dewetting).[35,36] In contrast solvent vapor annealing with n-hexane for both short and long periods of time had no noticeable effect on the morphology of the polymer film because the poly(styrene) does not absorb n-hexane and has no increased mobility. Therefore, as the solvent vapor composition shifts from mostly n-hexane to mostly THF one would expect to see a gradual change from a

mixed morphology to parallel cylinders for short annealing times and from a mixed morphology to parallel cylinders for long annealing times.

4.2 Solvent Vapor Composition Analysis

The solvent collection system was run for 36 hours, as described in Section 3.4, using THF as solvent A and n-hexane as solvent B. The nitrogen flowrate for both solvents was set to 8.5 mL/min. At the end of the run, approximately 10 µL of liquid solvent was collected in each of the vials. The liquid from each vial was dissolved in deuterated chloroform for ^{1}H-NMR analysis. The solvent composition was calculated by the integration of the n-hexane and THF peaks. A sample spectrum and resulting calculation is shown Figure 4.2-1 while the complete set of spectrums from the three runs are shown in the Appendix. The results from three runs are reported in Table 4.1-1 along with the average values for each chamber. The data show the expected trend of nearly pure n-hexane in chamber 1, nearly pure THF in chamber 6, with a gradient of compositions in chambers 2 through 5.

Table 4.1-1 Solvent vapor composition of each annealing chamber expressed in mole percent n-hexane when the THF and n-hexane volumetric flowrates were both set to 8.5 mL/min**.**

Chamber:	1	2	3	4	5	6
Run 1	99.4 %	92.1 %	72.2 %	62.9 %	33.0 %	2.0 %
Run 2	98.8 %	85.8 %	73.8 %	54.6 %	31.8 %	2.8 %
Run 3	99.7 %	82.9 %	74.4 %	49.1 %	33.3 %	13.4 %*
Average	99.3 %	86.9 %	73.5 %	55.5 %	32.7 %	2.5 %
Std. Dev.	0.5 %	4.7 %	1.1 %	6.9 %	0.8 %	0.6 %

*Data point determined to be an outlier and excluded from average and standard deviation calculations.

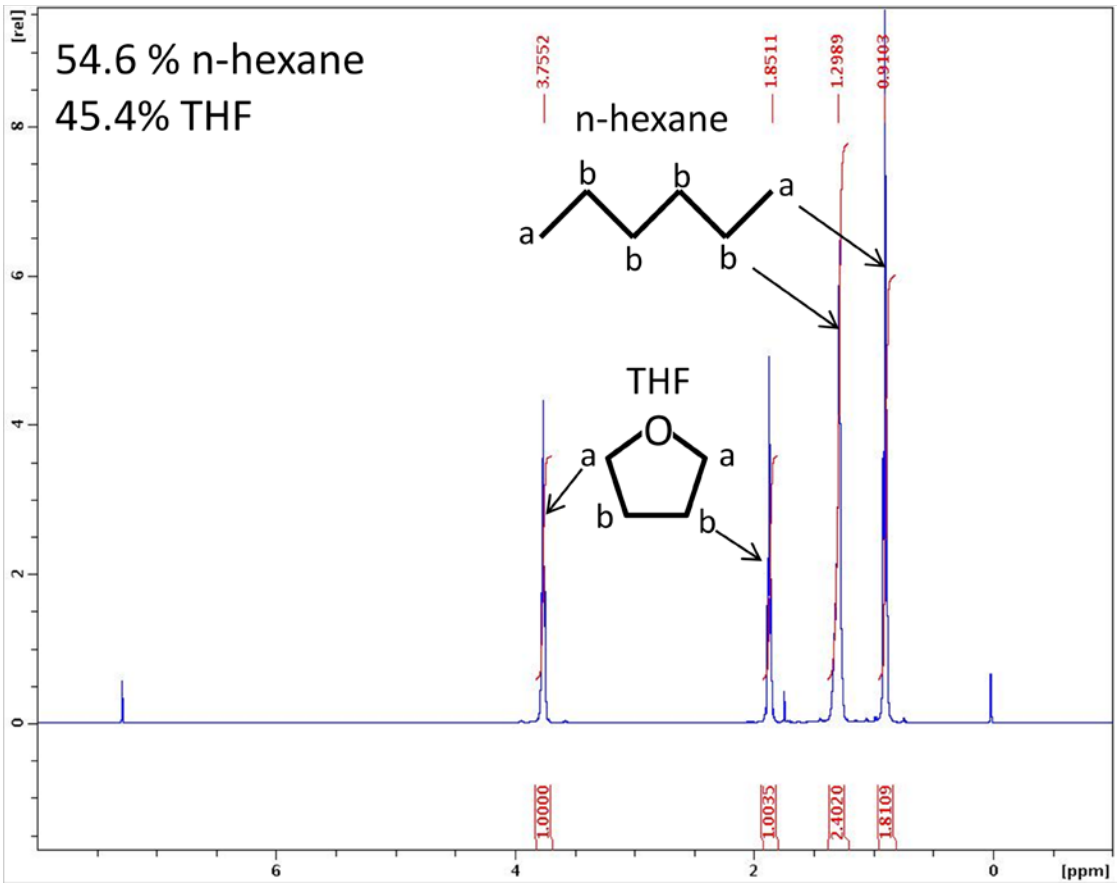

Figure 4.2-1 Sample ^{1}H-NMR analysis of solvent collected. Peak positions and integrated peak areas are shown above and below each peak respectively. Component mole fractions calculated from relative integrated areas under the THF and n-hexane curves. Curves a and b for n-hexane correspond to 6 and 8 protons respectively while curves a and b for THF both correspond to 4 protons.

4.3 Solvent Annealing Results

The solvent annealing system was used as described in Section 3.3 with THF as solvent A and n-hexane as solvent B. A 1 hour anneal and a 19.5 hour anneal were performed using the same flowrates used during the solvent collection (8.5 mL/min for both the THF and n-hexane). AFM and optical microscopy were used to image the resulting film morphologies (see Figures 4.3-1 and 4.3-2).

Chambers 1-4 from the 1 hour anneal indicate that as the solvent composition shifts from n-hexane to THF the long range order of the parallel cylinders increase. Chamber 5 shows the breaking of the parallel cylinders as the film begins to transition to perpendicular cylinders while chamber 6 shows the complete breaking of the parallel cylinders as the cylinders are in the middle of transitioning. Chamber 7 contains a mixture of parallel and perpendicular cylinders similar in representation to a non-annealed film.

Chamber 1 from the 19.5 hour anneal clearly demonstrates perpendicular cylinders with a few parallel cylinders remaining. Chambers 2-4 again illustrate that the film develops long range ordered parallel cylinders as the solvent vapor composition shifts from n-hexane to THF. The films in chambers 5 and 6 during the 19.5 hour anneal were dissolved from the high concentrations of THF present. The optical images show the residue of the film on the silicon substrate. Chamber 7 contains a mixture of parallel and perpendicular cylinders similar in representation to a non-annealed film.

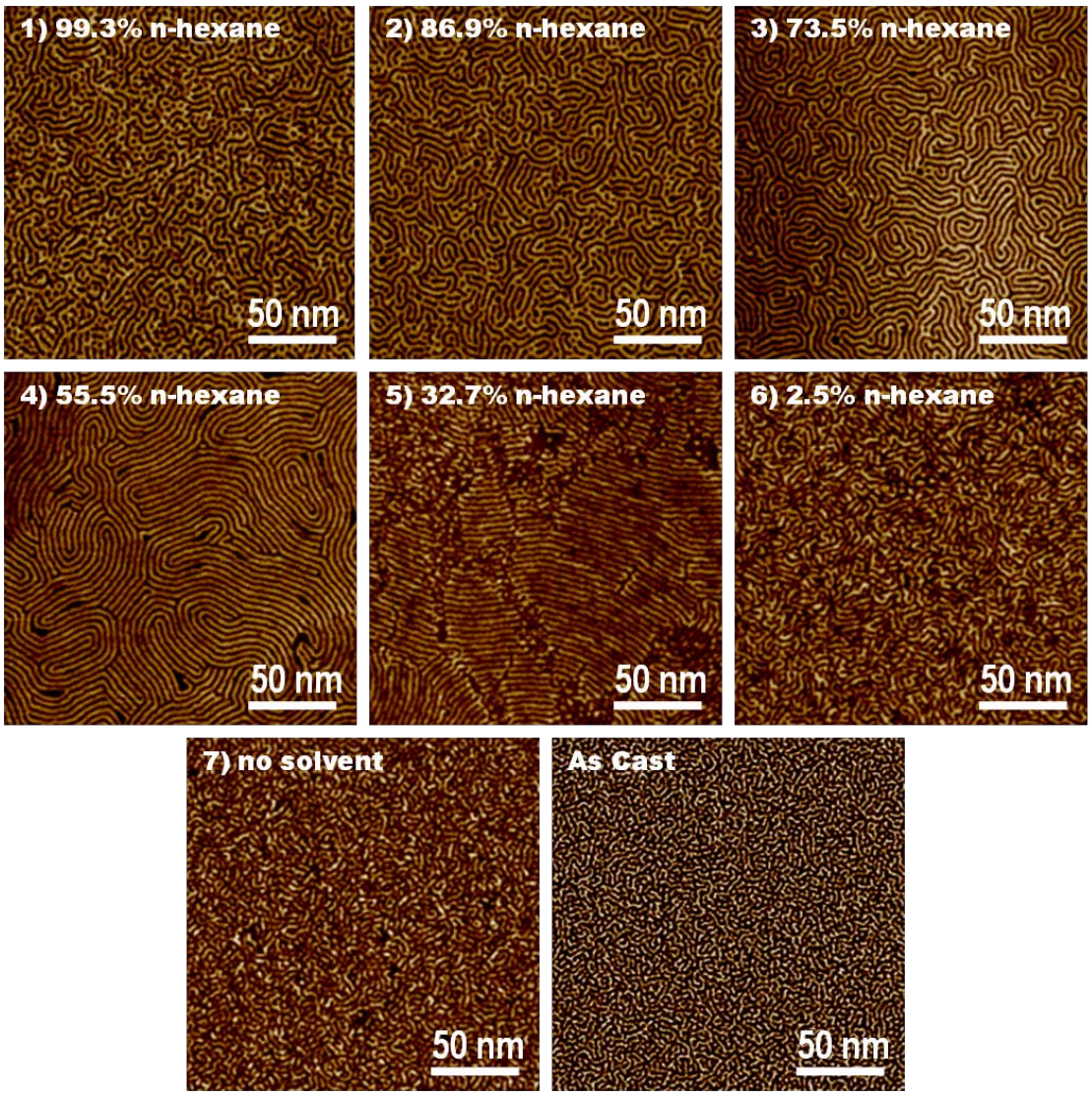

Figure 4.3-1 AFM images of an SIS film annealed for 1 hour using the microfluidic device with the THF and n-hexane flowrates both at 8.5 mL/min. Chamber numbers and solvent compositions are indicated on images. (1-4) Images show the transition from poorly ordered parallel cylinders to well ordered parallel cylinders as the mole percent of n-hexane decreases (THF increases). (5) Parallel cylinders break apart as they begin to flip from parallel to perpendicular from the decreasing concentration of n-hexane (increasing THF). (6) Parallel cylinders completely broken apart as they transition to perpendicular cylinders. (7) Mixture of parallel and perpendicular cylinders formed during flowcoating. Confirms that solvent cannot diffuse through the device. (As Cast) Representative AFM image of an as cast SIS film

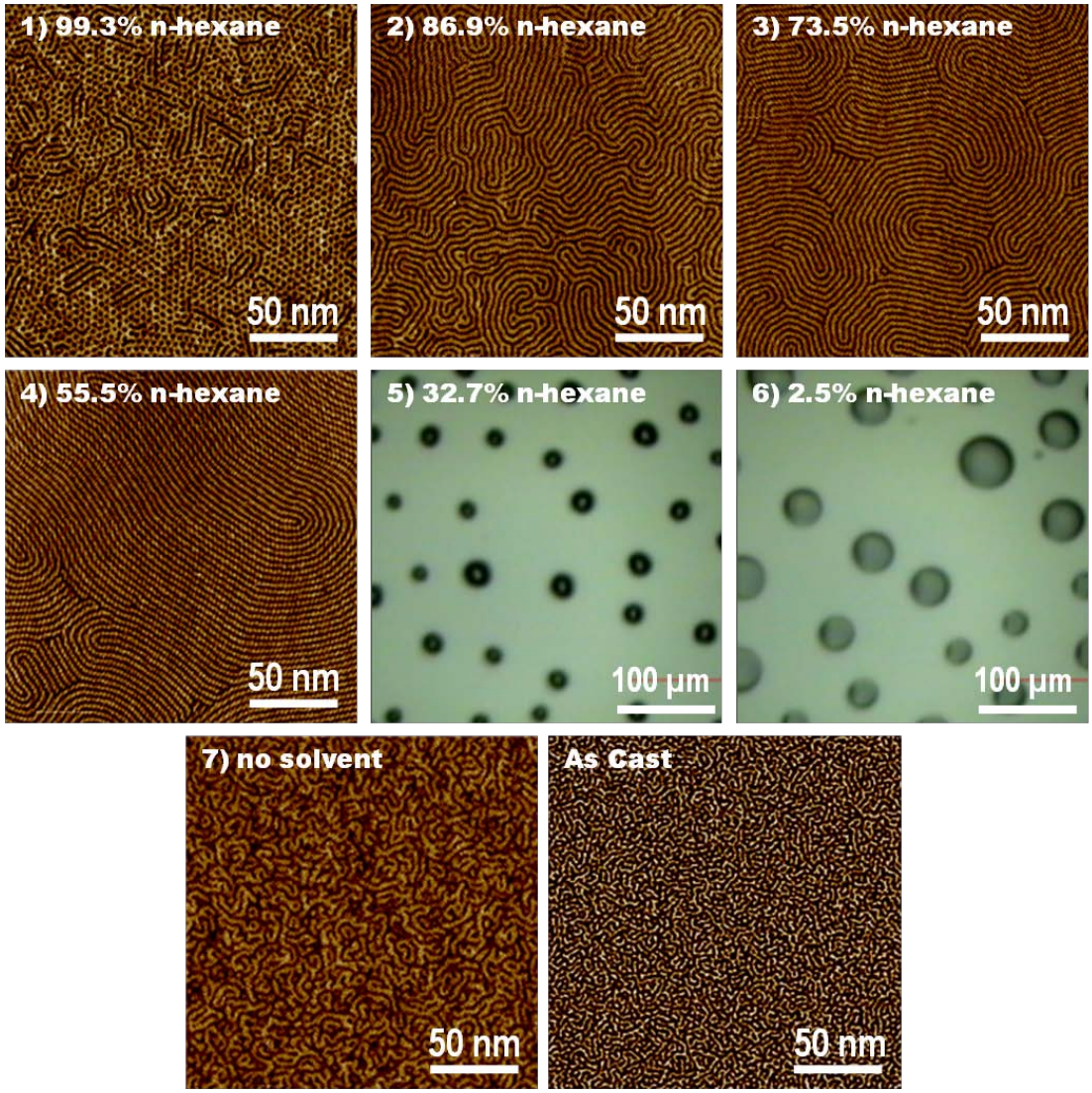

Figure 4.3-2 AFM and optical microscopy images of an SIS film annealed for 19.5 hours using the microfluidic device with the THF and n-hexane flowrates both at 8.5 mL/min. Chamber numbers and solvent composition are indicated on the images. (1-4) Images show the transition from perpendicular cylinders to well ordered parallel cylinders as the mole percent of n-hexane decreases (THF increases). (5-6) Polymer film dewet from the long exposure to high concentrations of THF (low concentrations of n-hexane). (7) Mixture of parallel and perpendicular cylinders formed during flowcoating. Confirms that solvent cannot diffuse through the device. (As Cast) Representative AFM image of an as cast SIS film

The resulting morphologies from both the long and short microfluidic device anneals show the expected pattern of a gradual transition from a mixed morphology to parallel cylinders with dewetting occurring after an extend period of time. The broken parallel cylinders observed in chambers 5 and 6 in the short anneal are indicative of the polymer film losing order as it begins to dewet. The perpendicular cylinders observed in chamber 1 of the long anneal were unexpected. It appeared that the small amount of THF that was present in the solvent vapor was enough to provide mobility to the styrene blocks, facilitating ordering. The resulting perpendicular cylinders are likely the result of the high concentration of n-hexane mitigating the poly(styrene)-poly(isoprene) interactions to the point where the energetics appeared neutral to each block. A comparison of the morphology in chamber 7 of both anneals to the representative as cast morphology as well as the morphology found in chamber 6 indicates that the solvent is unable to penetrate through the walls of the device.

Chapter 5

CONCLUSIONS AND FUTURE WORK

5.1 Conclusions

A procedure was successfully developed for the design, fabrication, and testing of solvent resistant microfluidic devices. The solvent collection procedure allows for the analysis of the solvent vapor composition in each chamber during an anneal. The solvent annealing of an SIS film using THF and n-hexane demonstrated the ability of the microfluidic device to perform high throughput anneals. The resulting morphologies from the anneals followed the expected trend of shifting from a mixed morphology to parallel cylinders as the solvent vapor composition shifted from n-hexane to THF. Analysis of the control chamber indicated that solvent is unable to penetrate the walls of the device.

5.2 Future Work

A process for measuring the thickness of the polymer film in each chamber as it swells with solvent during an anneal using the microfluidic device is being explored. The method for achieving this goal is to replace the top glass slide with a quartz slide, cut holes from the top down to each chamber, and use spectral reflectance to measure the film thickness. Current challenges include the calibration of the spectral reflectometer to operate through the quartz disk and the development of a method for measuring the thickness in each chamber in rapid succession. Achieving this goal will allow us to explore the effects of film thickness while simultaneously

studying the effects of solvent composition on block copolymer thin film self-assembly.

After exploring the effects of n-hexane and THF on SIS, the microfluidic device will be used to explore the effects of other solvents on SIS and other block copolymer systems. The goal is to develop a facile method for creating a library that will detail the effects of solvent composition on different block copolymer systems for determining the appropriate solvent annealing conditions to produce a desired morphology.

REFERENCES

1. Bates, F. S. (1991). *Science*. **251**(4996): 898-905.
2. Bates, F.S. and Frederickson, G. H. (1999) *Physics Today.* **52** 32-38
3. Segalman, R. A. (2005). *Materials Science and Engineering: R: Reports* **48**(6): 191-226.
4. Ruiz, R. *et al., Science* (2008) **321**, 936-939
5. Park, M. *et al., Science* (1997) **276**, 1401-1404
6. Pai, R. A. *et al., Science* (2004) **303**, 507-510
7. Hayward, R. C. *et al., Adv. Mater.* (2005) **17**, 2591-2595
8. Thurn-Albrecht, T. *et al., Adv. Mater.* (2000) **12**, 797-791
9. Olson, D. A. *et al., Chem. Mater.* (2007) **20**, 869-890
10. Yang, S. Y. *et al., Adv. Mater.* (2006) **18**, 709-712
11. Phillip, W. A. *et al., Appl. Mater. Interfaces* (2010) **2**, 847-853
12. Smith, A. P. *et al., Phys. Rev. Lett.* (2001) **87**.
13. M. W. Matsen, M. Schick, Phys. Rev. Lett. 72, 2660 (1994); M. W. Matsen, M. Schick, Macromolecules 27, 6761 (1994); 27, 7157 (1994). M. W. Matsen, F. S. Bates, Macromolecules, 29, 1091 (1996)
14. Han, E. *et al., Macromolecules* (2009) **42**, 4896-4901.
15. Mansky, P. *et al., Phys. Rev. Lett.* (1997) **79**, 237.
16. Knoll, A. *et al., J. Chem. Phys.* (2004) **120**, 1105-1116.
17. Kim, S. H. *et al., Adv. Mater.* (2004) **16**, 226-231.

18. Zettl, U. *et al., Langmuir* (Dec. 22, 2009 Article ASAP).

19. Di, Z. *et al., Macromolecules* (2009) **43**, 418-427.

20. Xuan, Y. *et al., Macromolecules* (2004) **37**, 7301-7307.

21. Lin, Z. Q. *et al., Adv. Mater.* (2002) **14**, 1373-1376.

22. Jung, Y. S. and Ross, C. A. *Adv. Mater.* (2009) **21**, 2540-2545.

23. Chen, Y. *et al., Langmuir* (2004) **20**, 3805-3808.

24. Li, Y. *et al., J. Phys. Chem. B* (2009) **114**, 1264-1270.

25. Bang, J. *et al., Macromolecules* (2007) **40**, 7019-7025.

26. Cavicchi, K. A. *et al., Polymer* (2005) **46**, 11635-11639.

27. Knoll, A. *et al., Phys. Rev. Lett.* (2002) **89**, 035501.

28. Cavicchi and Russell (2007) *Macromolecules.* **40**: 1181-1186

29. Fasolka and Mayes (2001) *Annu. Rev. Mater. Res*. **31**: 323–55

30. Cabral et al. (2004) *Langmuir.* **20**: 10020-10029

31. Harrison et al. (2004) *J. Micromoch. Microeng*. **14**: 153–158

32. Cramer et al. (2004) *J. Polymer Science Part A: Polymer Chemistry*. **42** 1752-1757

33. Roussel et al. (2002) *Eur. Phys. J.* E **8:** 283–288

34. Stafford, C. M. et al. (2006). *Review of Scientific Instruments.* **77**(2).

35. Epps, T. H. *et al., Langmuir* (2007) **23**, 3355-3362

36. Harant, A. W. and Bowman, C. N. (2005) *J Vac Sci Technol B Microelectron Nanometer Struct Process* **23**, 1615-1621.

37. Albert, J. N. L. and Epps, T. H. (2010) *Materials Today* (in press)

APPENDIX

A.1 ^{1}H-NMR Analysis of Solvent Collection Run 1

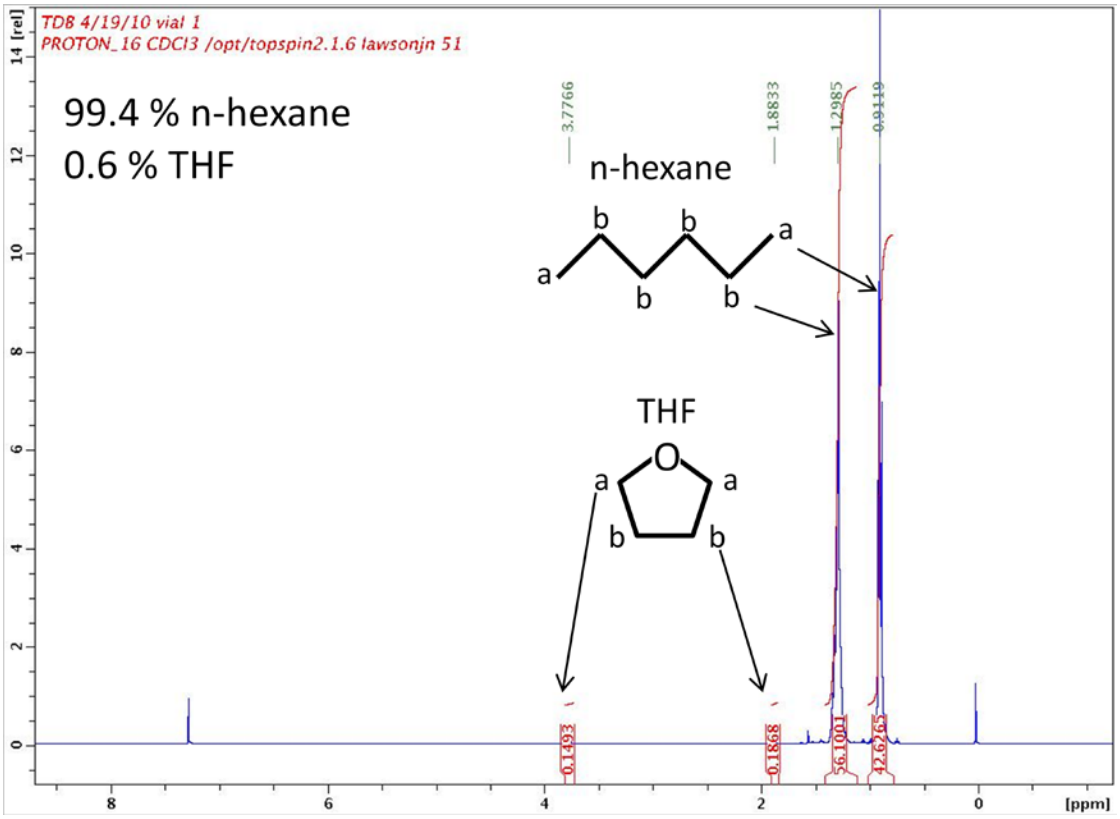

Figure A.1-1 ^{1}H-NMR analysis of solvent collected from chamber 1 during solvent collection run 1. Peak positions and integrated peak areas are shown above and below each peak respectively. Component mole fractions calculated from relative integrated areas under the THF and n-hexane curves.

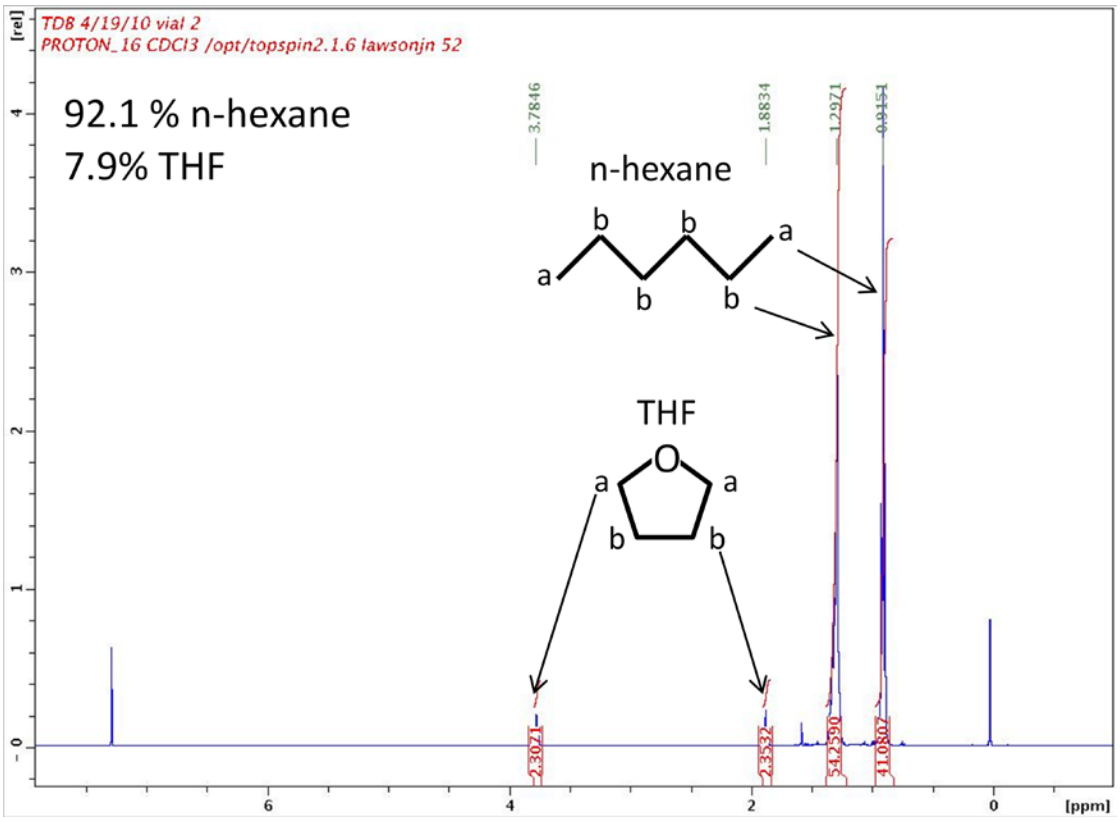

Figure A.1-2 ^{1}H-NMR analysis of solvent collected from chamber 2 during solvent collection run 1. Peak positions and integrated peak areas are shown above and below each peak respectively. Component mole fractions calculated from relative integrated areas under the THF and n-hexane curves.

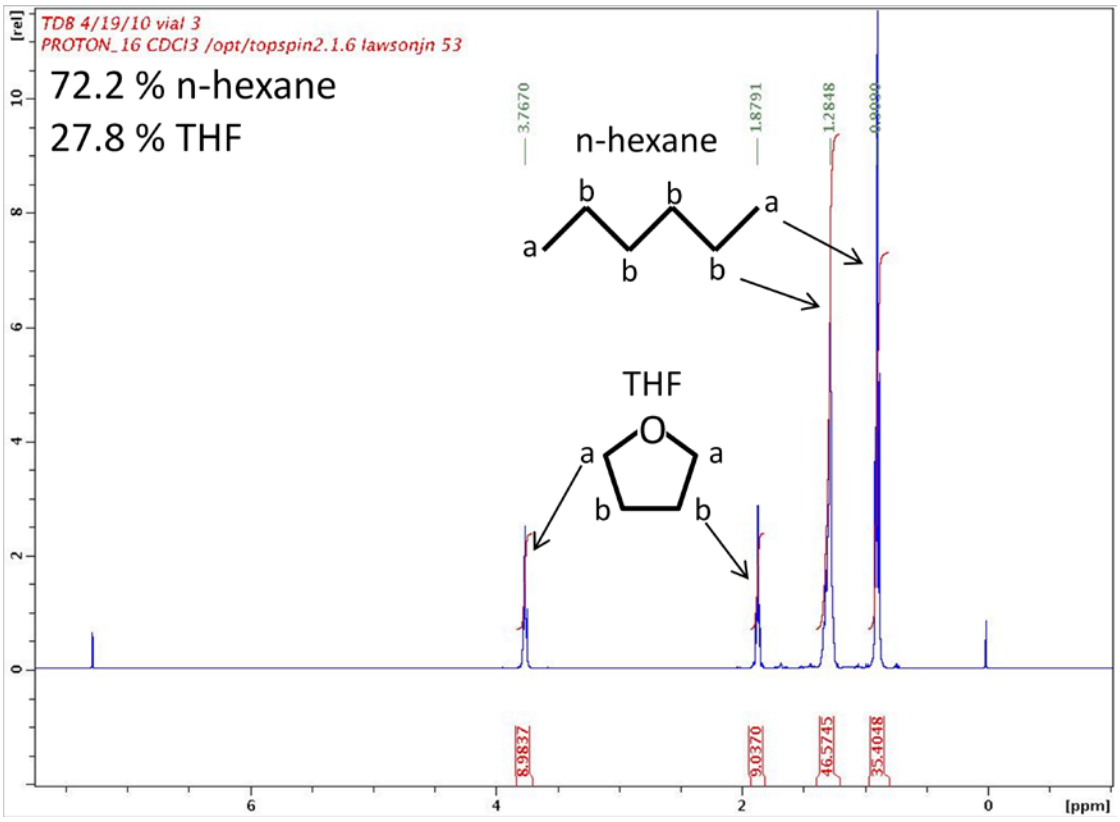

Figure A.1-3 ^{1}H-NMR analysis of solvent collected from chamber 3 during solvent collection run 1. Peak positions and integrated peak areas are shown above and below each peak respectively. Component mole fractions calculated from relative integrated areas under the THF and n-hexane curves.

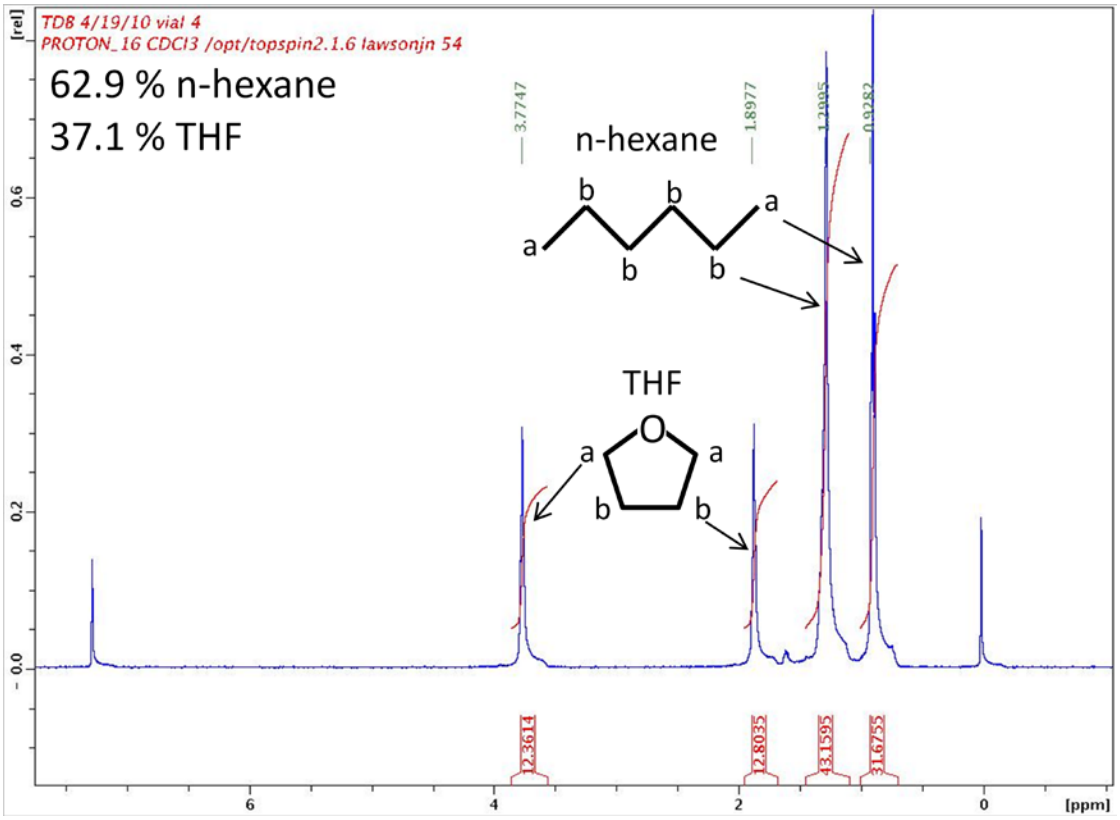

Figure A.1-4 [1]H-NMR analysis of solvent collected from chamber 4 during solvent collection run 1. Peak positions and integrated peak areas are shown above and below each peak respectively. Component mole fractions calculated from relative integrated areas under the THF and n-hexane curves.

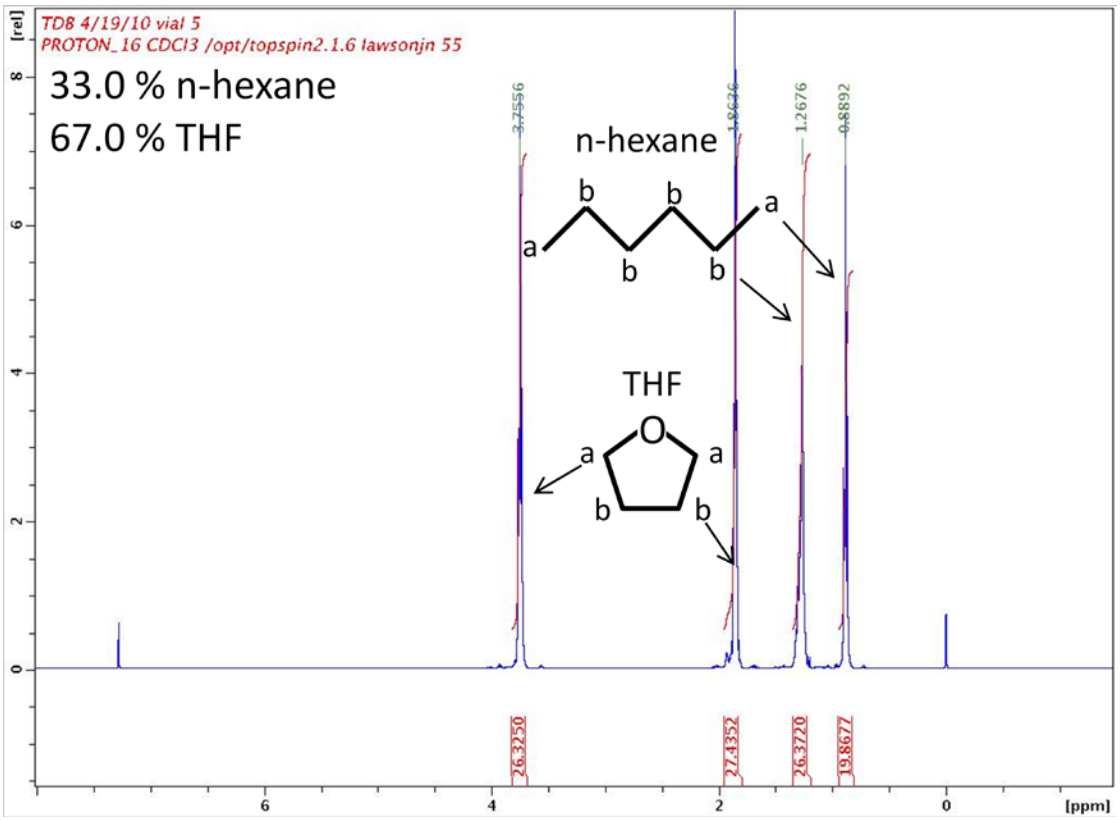

Figure A.1-5 ^{1}H-NMR analysis of solvent collected from chamber 5 during solvent collection run 1. Peak positions and integrated peak areas are shown above and below each peak respectively. Component mole fractions calculated from relative integrated areas under the THF and n-hexane curves.

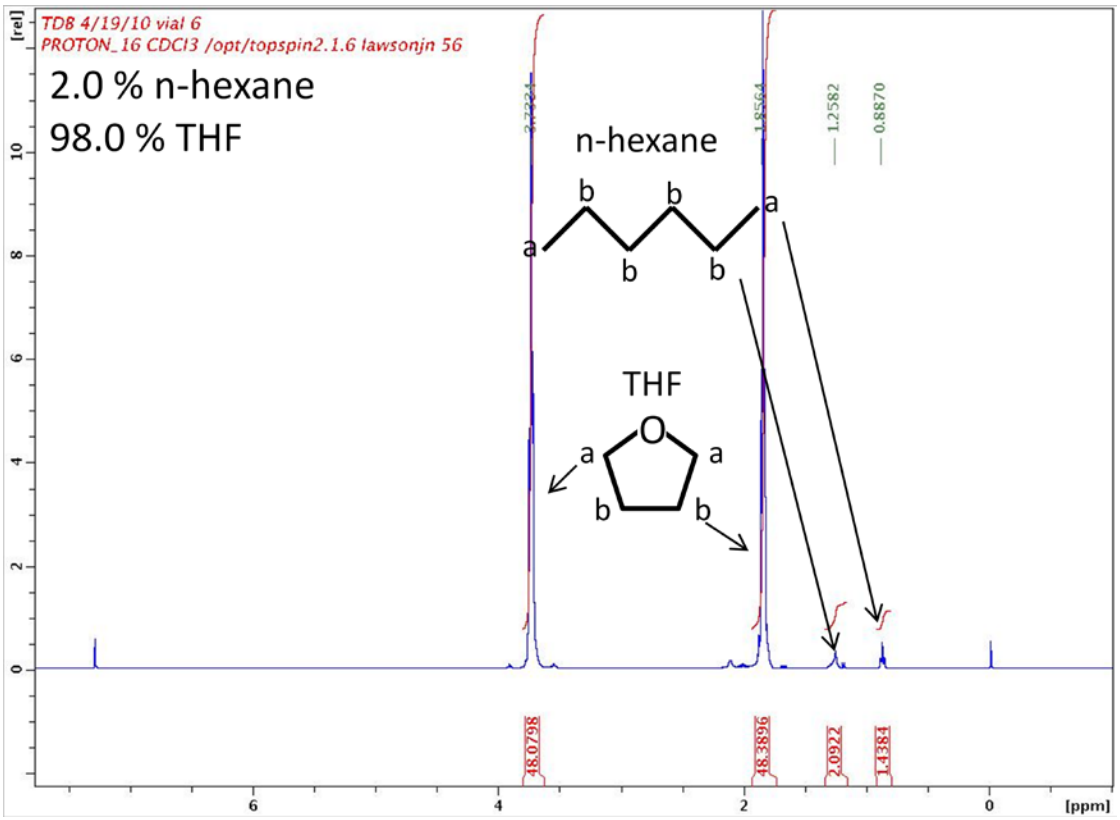

Figure A.1-6 ^{1}H-NMR analysis of solvent collected from chamber 6 during solvent collection run 1. Peak positions and integrated peak areas are shown above and below each peak respectively. Component mole fractions calculated from relative integrated areas under the THF and n-hexane curves.

A.2 ^{1}H-NMR Analysis of Solvent Collection Run 2

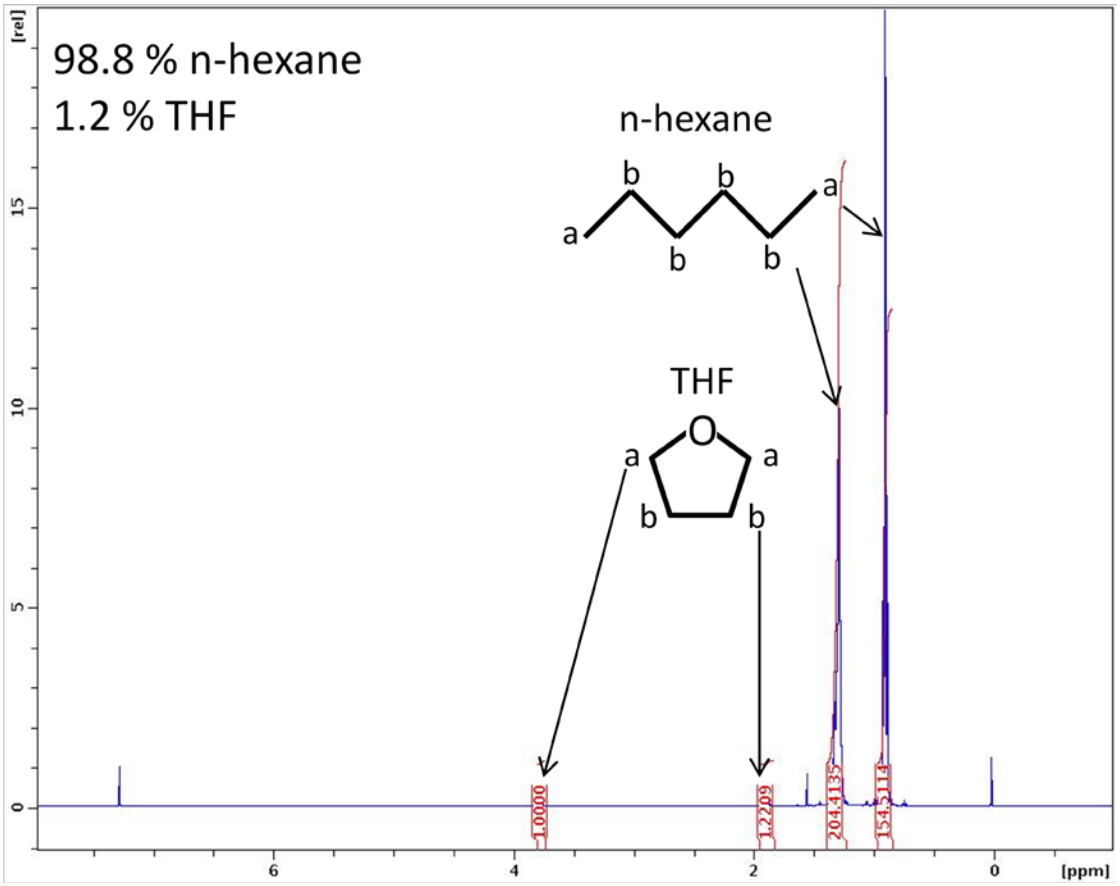

Figure A.2-1 ^{1}H-NMR analysis of solvent collected from chamber 1 during solvent collection run 2. Peak positions and integrated peak areas are shown above and below each peak respectively. Component mole fractions calculated from relative integrated areas under the THF and n-hexane curves.

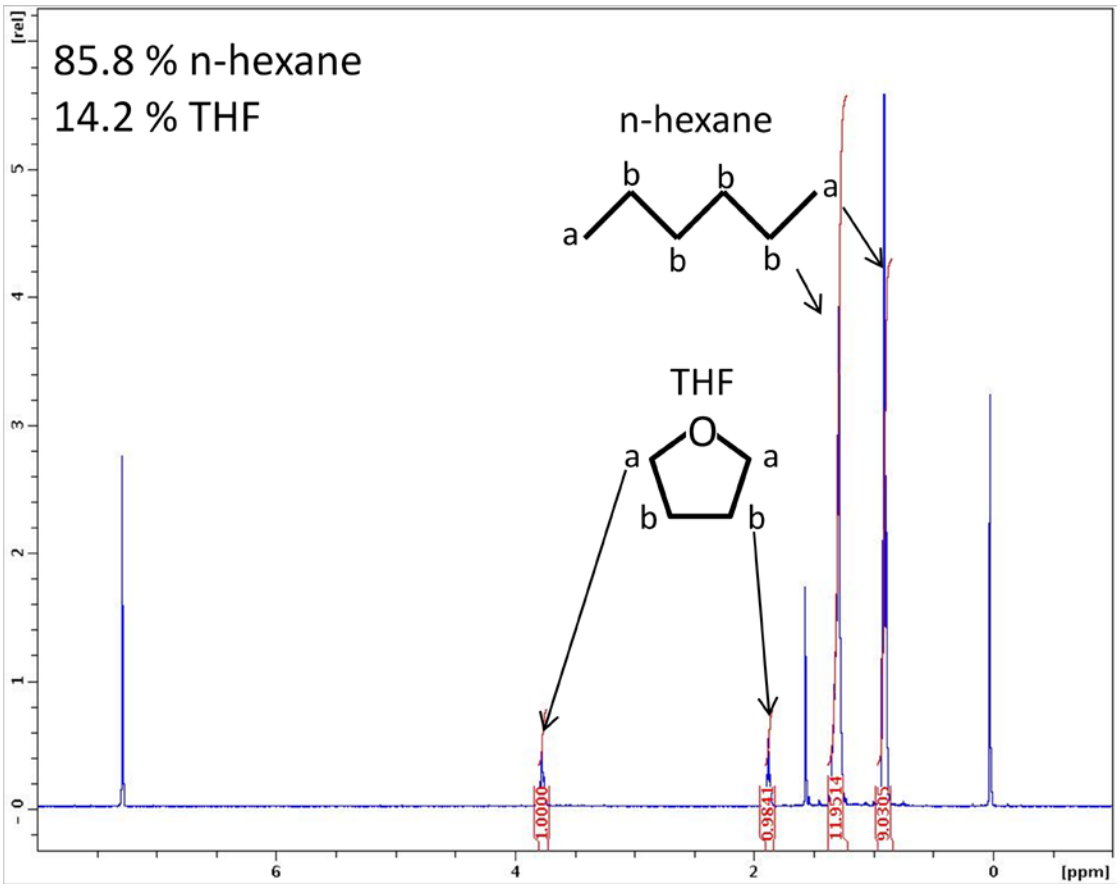

Figure A.2-2 ^{1}H-NMR analysis of solvent collected from chamber 2 during solvent collection run 2. Peak positions and integrated peak areas are shown above and below each peak respectively. Component mole fractions calculated from relative integrated areas under the THF and n-hexane curves.

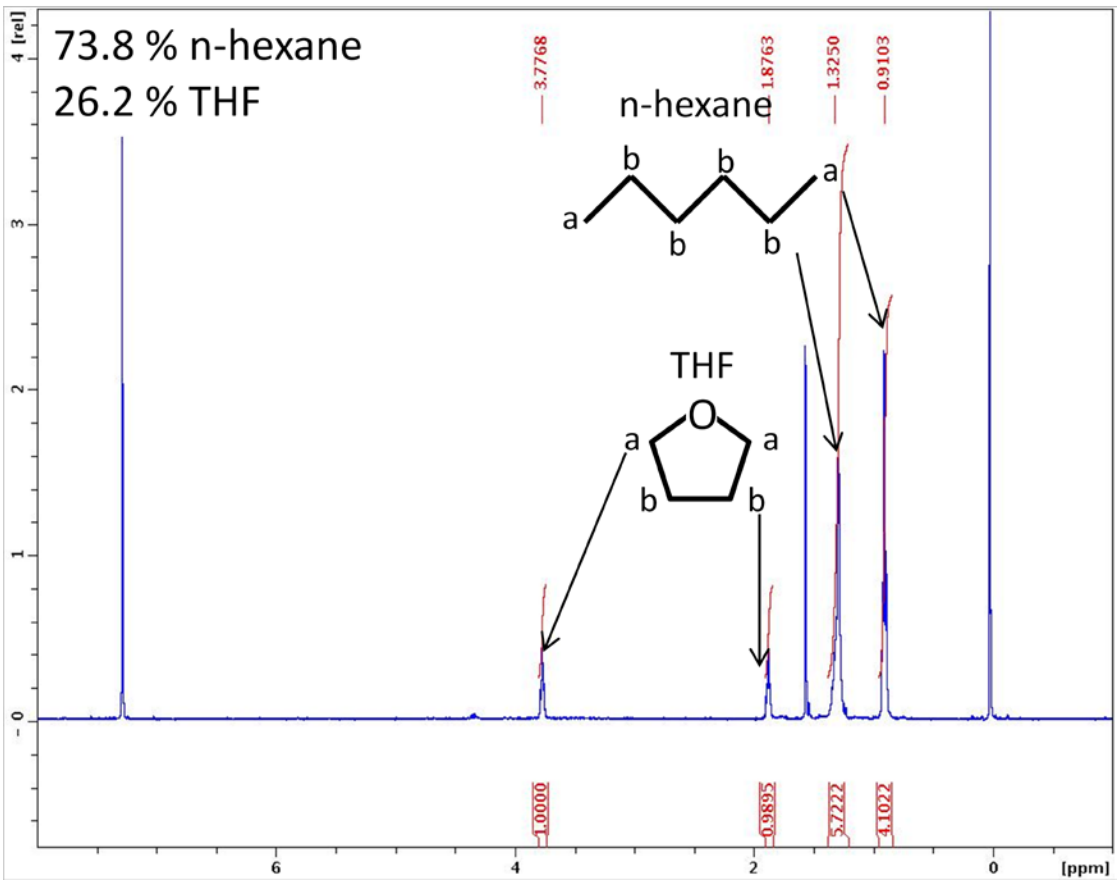

Figure A.2-3 ^{1}H-NMR analysis of solvent collected from chamber 3 during solvent collection run 2. Peak positions and integrated peak areas are shown above and below each peak respectively. Component mole fractions calculated from relative integrated areas under the THF and n-hexane curves.

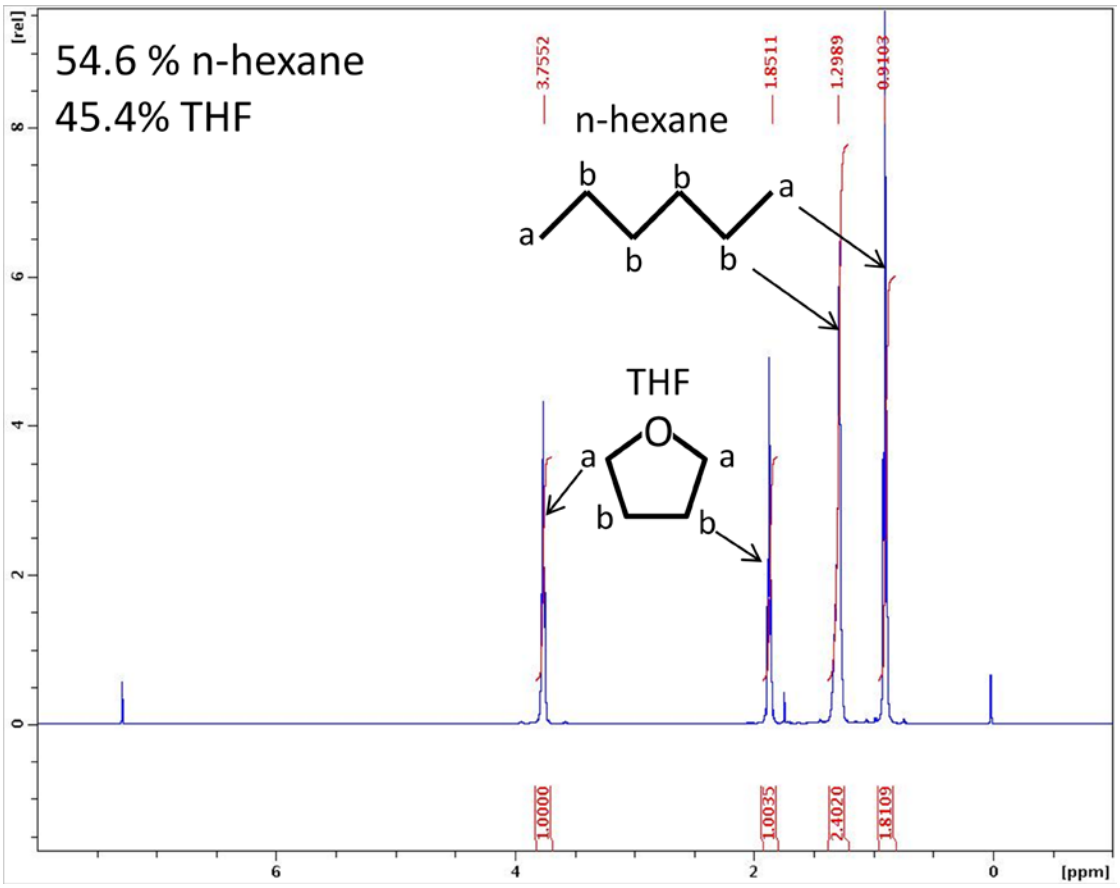

Figure A.2-4 ^{1}H-NMR analysis of solvent collected from chamber 4 during solvent collection run 2. Peak positions and integrated peak areas are shown above and below each peak respectively. Component mole fractions calculated from relative integrated areas under the THF and n-hexane curves.

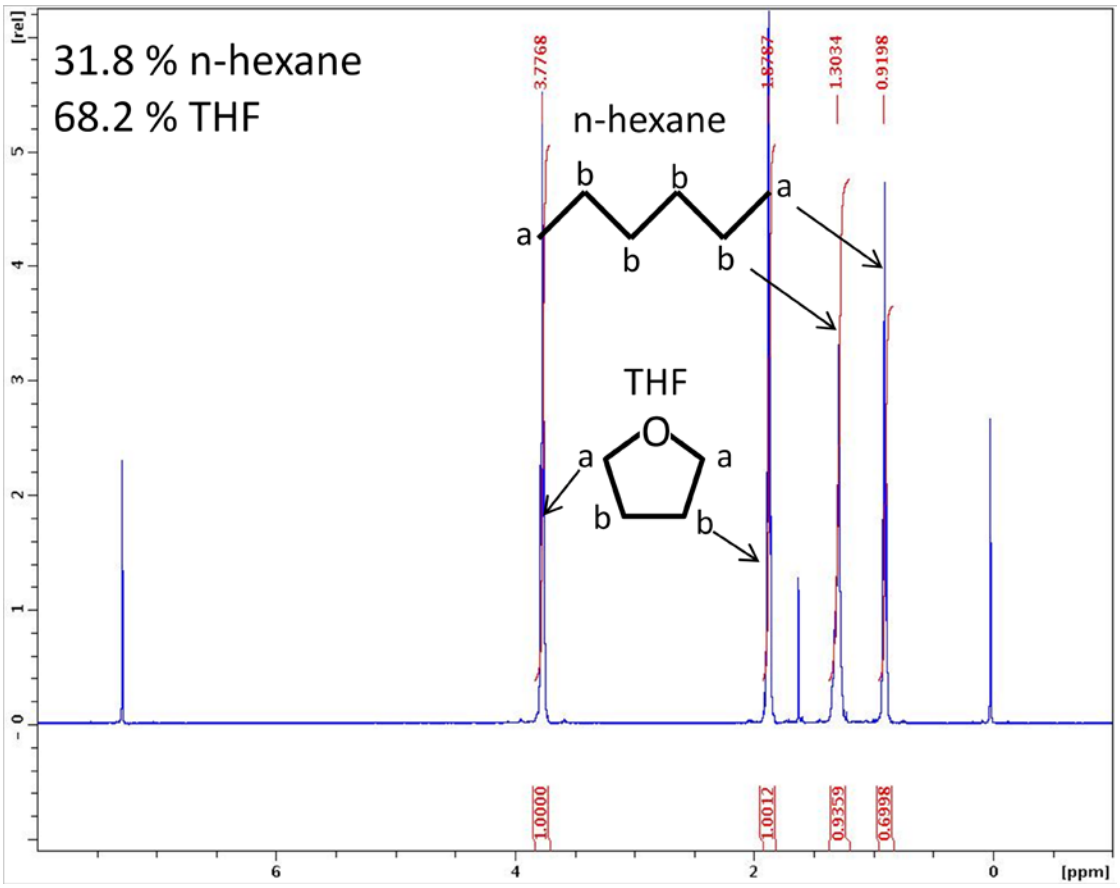

Figure A.2-5 ^{1}H-NMR analysis of solvent collected from chamber 5 during solvent collection run 2. Peak positions and integrated peak areas are shown above and below each peak respectively. Component mole fractions calculated from relative integrated areas under the THF and n-hexane curves.

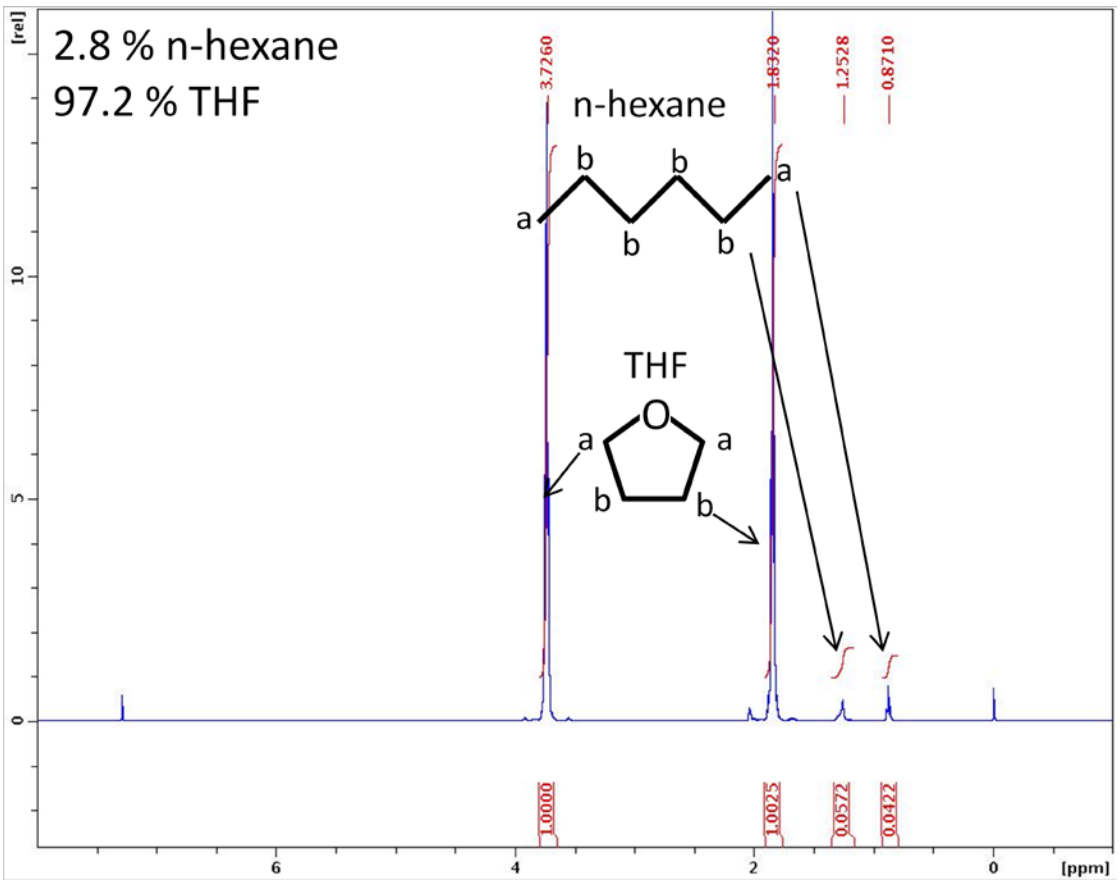

Figure A.2-6 ^{1}H-NMR analysis of solvent collected from chamber 6 during solvent collection run 2. Peak positions and integrated peak areas are shown above and below each peak respectively. Component mole fractions calculated from relative integrated areas under the THF and n-hexane curves.

A.3 ^{1}H-NMR Analysis of Solvent Collection Run 3

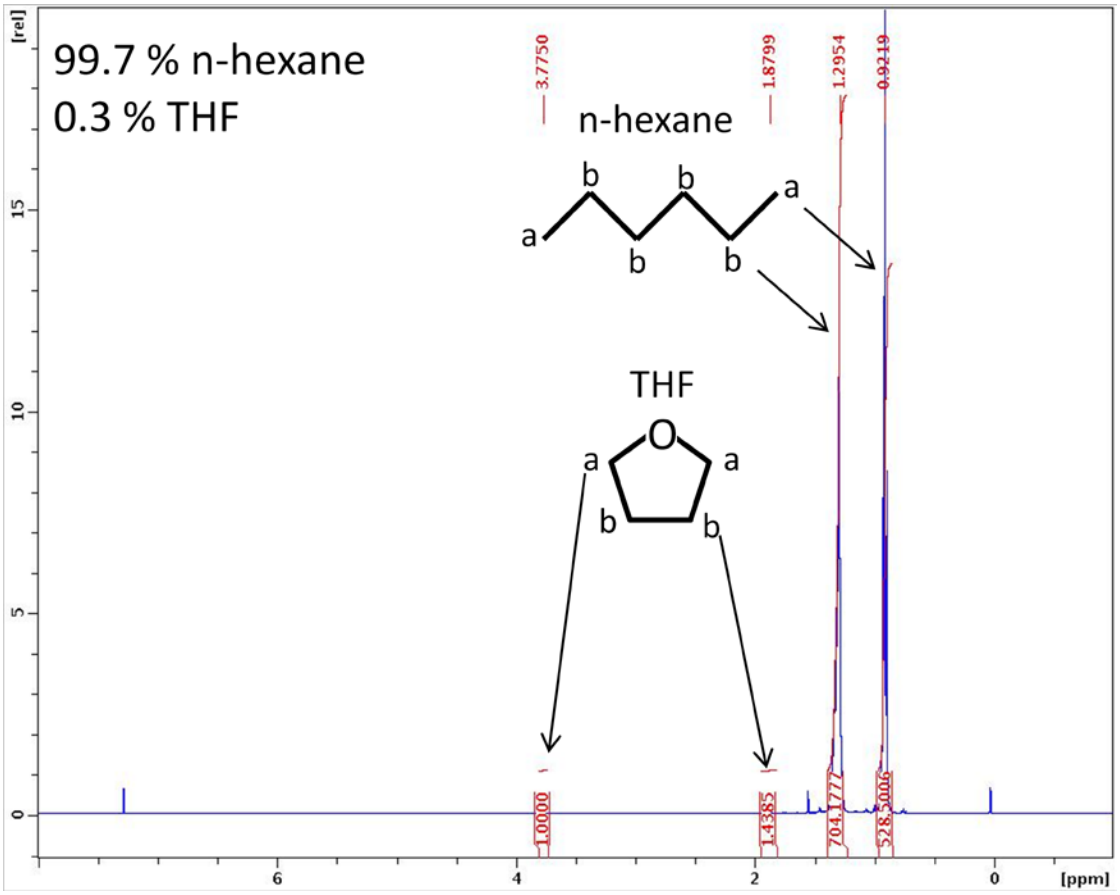

Figure A.3-1 ^{1}H-NMR analysis of solvent collected from chamber 1 during solvent collection run 3. Peak positions and integrated peak areas are shown above and below each peak respectively. Component mole fractions calculated from relative integrated areas under the THF and n-hexane curves.

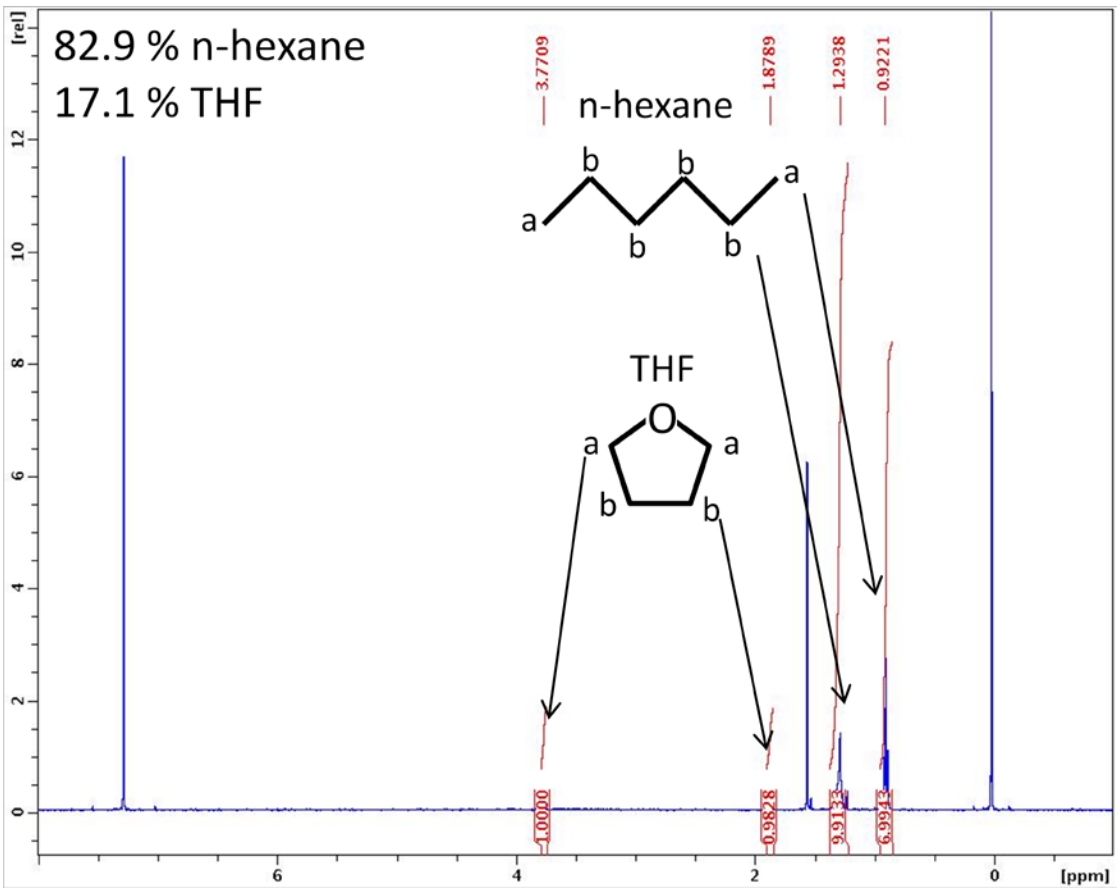

Figure A.3-2 [1]H-NMR analysis of solvent collected from chamber 2 during solvent collection run 3. Peak positions and integrated peak areas are shown above and below each peak respectively. Component mole fractions calculated from relative integrated areas under the THF and n-hexane curves.

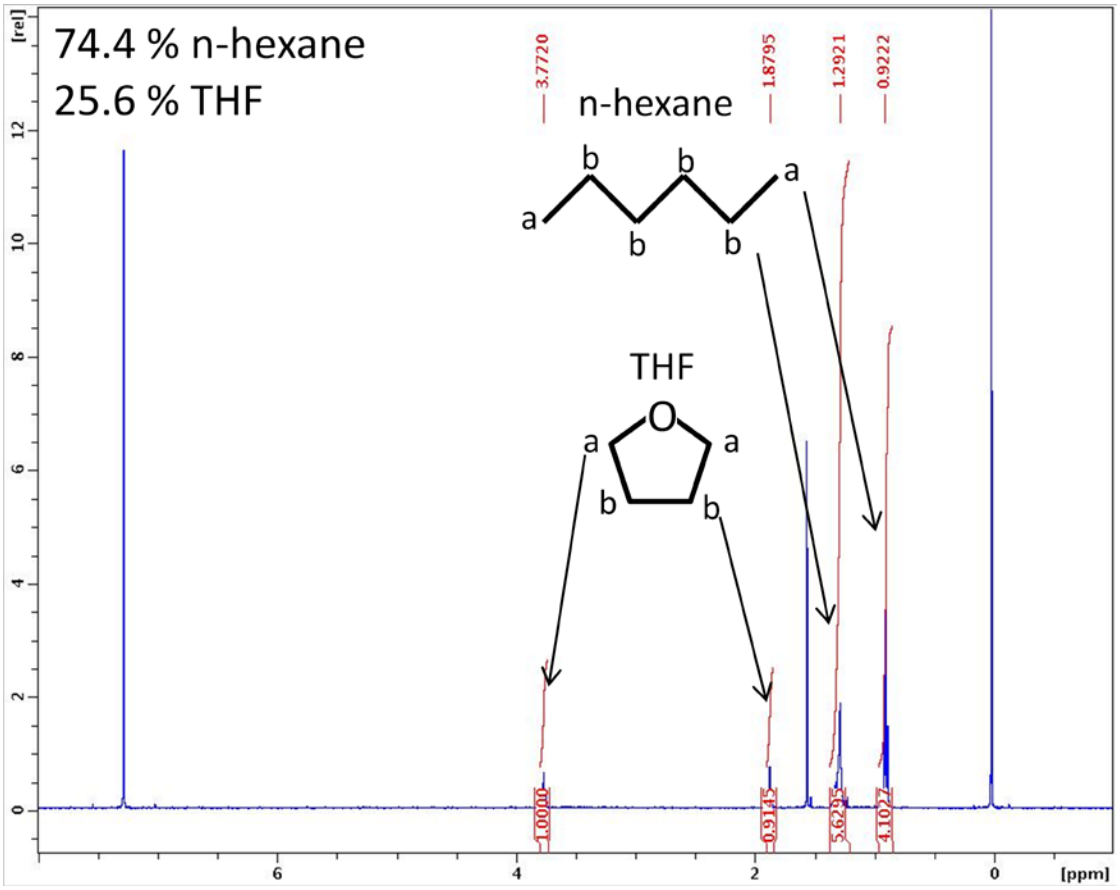

Figure A.3-3 [1]H-NMR analysis of solvent collected from chamber 3 during solvent collection run 3. Peak positions and integrated peak areas are shown above and below each peak respectively. Component mole fractions calculated from relative integrated areas under the THF and n-hexane curves.

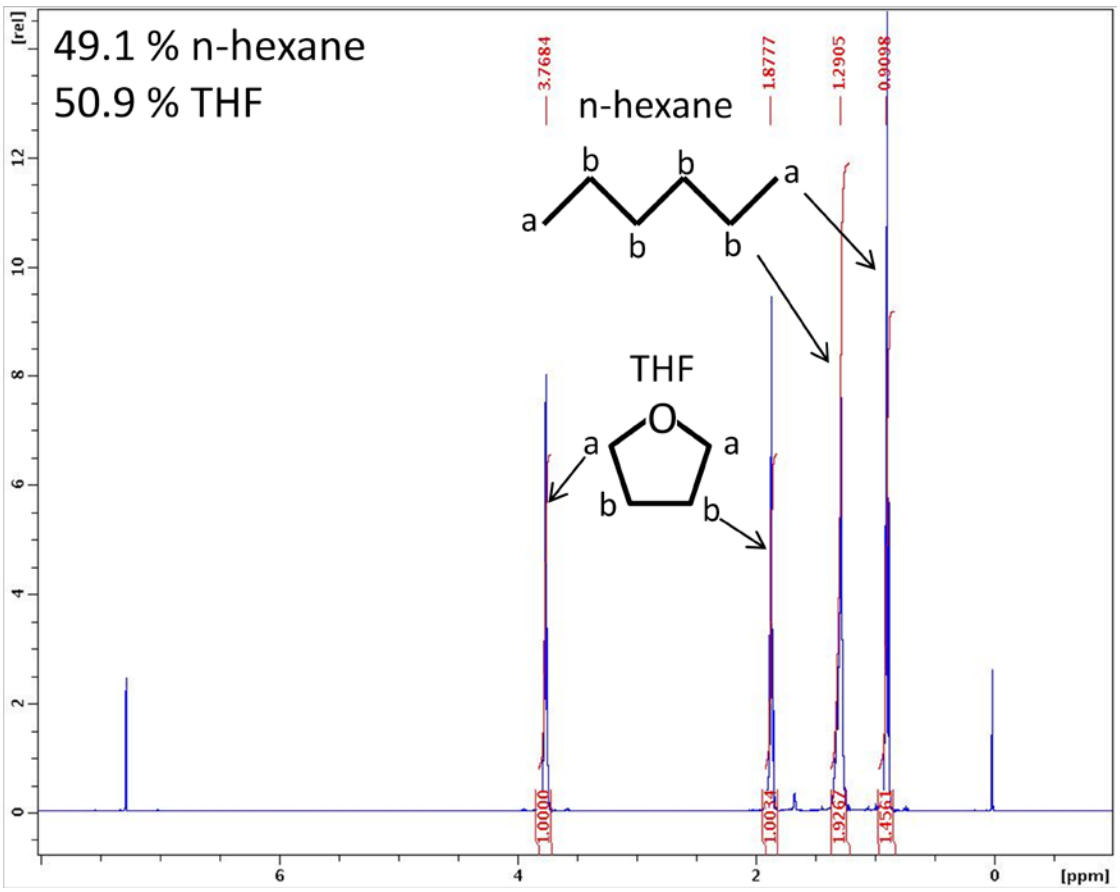

Figure A.3-4 [1]H-NMR analysis of solvent collected from chamber 4 during solvent collection run 3. Peak positions and integrated peak areas are shown above and below each peak respectively. Component mole fractions calculated from relative integrated areas under the THF and n-hexane curves.

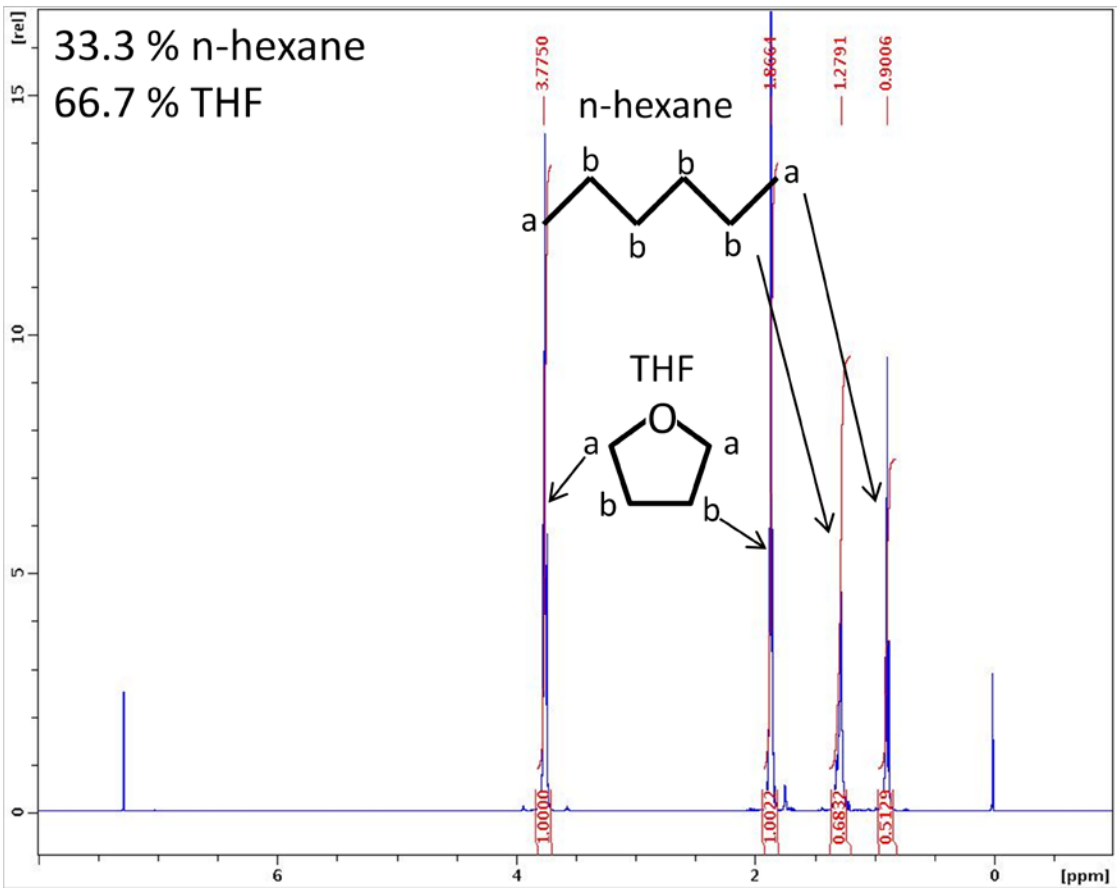

Figure A.3-5 ^{1}H-NMR analysis of solvent collected from chamber 5 during solvent collection run 3. Peak positions and integrated peak areas are shown above and below each peak respectively. Component mole fractions calculated from relative integrated areas under the THF and n-hexane curves.

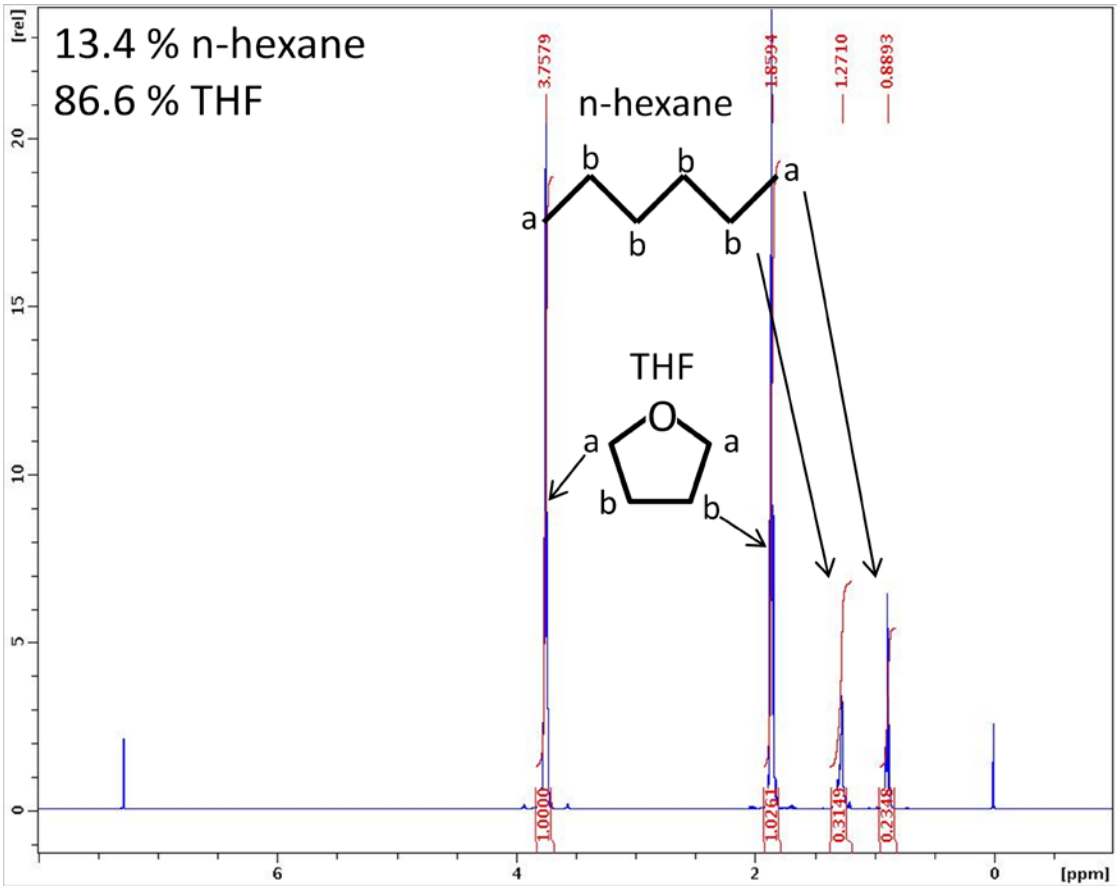

Figure A.3-6 [1]H-NMR analysis of solvent collected from chamber 6 during solvent collection run 3. Peak positions and integrated peak areas are shown above and below each peak respectively. Component mole fractions calculated from relative integrated areas under the THF and n-hexane curves.